Chapter 12

Ocean Surface Circulation

Nikolai Maximenko*, Rick Lumpkin† and Luca Centurioni‡

*International Pacific Research Center, School of Ocean and Earth Science and Technology, University of Hawaii at Manoa, Honolulu, Hawaii, USA

†Atlantic Oceanographic and Meteorological Laboratory, NOAA, Miami, Florida, USA

‡Scripps Institution of Oceanography, University of California, San Diego, La Jolla, California, USA

This chapter is dedicated to the memory of Peter Niiler.

Chapter Outline

1. OBSERVED NEAR-SURFACE CURRENTS

Ocean currents connect local basins into the single Global Ocean. Together with atmospheric circulation, they serve to maintain the planetary balance of heat and freshwater. Currents are hard to measure. It required decades of international effort and generations of scientists and engineers before the observational network was built that monitors today's surface currents globally and in near real time.

1.1. Global Drifter Program and History of Lagrangian Observations

For many centuries, the large-scale pattern of ocean currents was inferred from the downstream fate of flotsam and debris of identifiable origin (c.f., Sverdrup et al., 1942). This information could be combined with *in situ* current estimates from ship drift—derived from the difference between the absolute motion of a ship and its relative motion through the water—to create maps of ocean currents and transport pathways. However, the speed of ocean surface currents can only be poorly estimated from this approach. Without robust knowledge of travel times and exact pathways, flotsam does not provide this information; ship drift in the pre-Global Positioning System (pre-GPS) period could suffer from relatively large navigational errors, resulting in surface current errors of O (20 cm s^{-1}) (Richardson and McKee, 1984). In addition, the force of the wind on a ship is not negligible, creating systematic biases in regions of large-scale, persistent winds such as the Trades or Westerlies (Richardson and Walsh, 1986; Reverdin et al., 1994; Lumpkin and Garzoli, 2005).

To reduce the effect of wind forcing on surface current measurements, investigators developed Lagrangian drifting buoys (or drifters) that had a small drag area above the waterline compared to the drag area below. They did this by attaching a sea anchor, or drogue, to the floating surface buoy. In the presatellite era, the drifter's position was determined by triangulation from a fixed point (land or an anchored ship). Observations of drogued drifters were collected as early as the mid-1700s off the US northeast coast (Franklin, 1785; Davis, 1991) and worldwide in the *Challenger* oceanographic survey of 1872–1876 (Thomson, 1877; Niiler, 2001).

Ocean Circulation and Climate, Vol. 103. http://dx.doi.org/10.1016/B978-0-12-391851-2.00012-X

With the introduction of radio, visual observations were no longer necessary to track drifters. Drifters with radio transmissions could be tracked via triangulation from shore receivers or from aircraft, allowing for larger arrays and observations in harsher conditions. This technology was used in the US Coastal Ocean Dynamics Experiment (CODE) of 1981–1982, in which 164 radio-tracked drifters were deployed off the US west coast (Davis, 1985a). These CODE drifters (also known as "Davis" drifters) had four cruciform-shaped drogue panels centered at a depth of ~60 cm beneath the surface, attached to a central vertical tube that contained the transmitter, batteries, and antenna (Davis, 1985a). Four floats at the upper, outer corners of each drogue panel provided additional buoyancy.

In the 1970s, satellites opened the possibility of worldwide drifter measurements. In the pre-GPS (mid-1990s) era, drifter positions were determined from the Doppler shift of the drifter's transmissions as measured by the satellite; the most prominent example of this technique is the Argos system created by the US agencies National Oceanic and Atmospheric Administration (NOAA) and National Aeronautics and Space Administration (NASA) and the French space agency Centre National d'Etudes Spatiales (CNES) and operated by Collecte Localisation Satellites (CLS) in Toulouse, France. Most of the modern drifters are tracked by the Argos system. In recent years, a growing number of data buoys are taking advantage of the Iridium satellite network to relay data globally, with GPS for positioning.

Several independent groups developed and deployed Argos-tracked drifters starting in the 1970s, leading to a number of competing designs for the instrument. In 1975, as part of the North Pacific Experiment (NORPAX), 165 drifters were released which were 3 m tall, 38 cm-diameter cylinders, most drogued at 30 m with a 9 m-diameter parachute (McNally et al., 1983). In 1976–1978, an array of 35 drifters, drogued at 200 m with either a 25 kg weight or a "window shade" drogue (a flat panel, usually weighted at the bottom), was deployed in the Gulf Stream region (Richardson, 1980). These drifters included a tether strain sensor to indicate drogue presence, but this sensor often failed shortly after deployment (Richardson, 1980). A large array of over 300 drifters was deployed as part of the Global Atmosphere Research Program (GARP) First Global GARP Experiment (FGGE) in 1979–1980 in the Southern Ocean (Garrett, 1980). FGGE drifters were not all identical, but the majority had a 3.4-m surface float with 100 m line acting as a drogue, weighted at the end with 29.5 kg of chain (Pazan and Niiler, 2001). From 1981–1984, 113 "HERMES" drifters, drogued with a window shade at 100 m depth, were deployed in the eastern and northern North Atlantic (Krauss and Böning, 1987). In 1983–1985, 53 "TIROS" drifters were deployed in the tropical Atlantic as part of the programs Seasonal Response of the Equatorial Atlantic (SEQUAL) and Programme Français Océan et Climat dans l'Atlantique Équatorial (FOCAL). These drifters had a 20-m^2 window shade drogue at 20 m depth, or (for the "mini-TIROS") a 2.2-m^2 window shade drogue at 5 m depth (Richardson and Reverdin, 1987) and did not include a sensor to indicate drogue presence. In 1987–1988, two arrays totaling 77 Argos-tracked drifters were deployed off Point Arena, California, with rigid "tristar" drogues resembling a radar reflector centered at 15 m depth (Brink et al., 1991). An array of 49 of these drifters was also deployed off the coast of British Columbia in 1987 (Paduan and Niiler, 1993). In addition to these designs, the CODE drifter mentioned above was converted to satellite positioning and used in the Gulf of Mexico Surface Current Lagrangian Program (SCULP) deployments of 1993–1998 (LaCasce and Ohlmann, 2003).

It was clear by the early 1980s that a global array of drifters would be invaluable for oceanographic and climate research, but data from existing regional deployments could not be easily combined due to the disparate water-following characteristics of the various drifter designs (WCRP, 1988; Niiler, 2001). Logistical demands for creating and maintaining a global array also called for a design that was relatively inexpensive to manufacture and transport and easy to deploy. In 1982, the World Climate Research Program (WCRP) declared that a standardized drifter should be developed to meet these constraints (WCRP, 1988; Niiler, 2001). This development took place under the Surface Velocity Program (SVP) of the Tropical Ocean Global Atmosphere (TOGA) experiment and the World Ocean Circulation Experiment (WOCE). NOAA's Atlantic Oceanographic and Meteorological Laboratory (AOML; P.I. Donald Hansen), MIT's Draper Laboratory (P.I. John Dahlen), and the Scripps Institution of Oceanography (SIO; P.I. Peter Niiler) proposed competing designs for what was to become the Global Drifter Program (GDP) drifter. In 1985–1989, the water-following characteristics of a number of drogue designs were evaluated by attaching vector-measuring current meters to the tops and bottoms of the drogues (Niiler et al., 1987, 1995). Significant problems were identified with several of the drogue types: window shade drogues could twist at an angle and create a sailing force across a current; parachute drogues could collapse and subsequently provide very little drag; line-and-chain drogues (such as used in the FGGE drifters) provided too little drag area compared to the surface float, resulting in significant wind- and wave-driven slip with respect to the current at the drogue depth (Niiler et al., 1987, 1995; Niiler and Paduan, 1995; Pazan and Niiler, 2001). The radar reflector-shaped tristar drogue developed at SIO had somewhat lower slip than the holey-sock drogue developed at AOML (Niiler et al., 1995), but cost more and was more difficult to ship and deploy. By 1993, a design for the GDP drifter had emerged which combined the holey-sock drogue

of the AOML drifter, centered at a depth of 15 m beneath the ocean surface, with the reinforced tether ends and spherical surface float of the SIO drifter. This design (Sybrandy and Niiler, 1991) became the blueprint for future GDP drifter development.

The 1991 GDP drifter design was extremely robust, but was relatively expensive and heavy, with a surface float of 40 cm in diameter and a drogue of 6.44 m length, 92 cm in diameter and a total weight of 45 kg (Sybrandy and Niiler, 1991). A smaller, less-expensive redesign (Sybrandy et al., 1992) was introduced to reduce manufacturing and shipping costs, while retaining the same water-following characteristics. This 20 kg "mini" drifter has approximately one-third the manufacturing cost of the original design, has a smaller surface float, thinner tether, and smaller drogue (61 cm in diameter), while retaining the ratio of the drag area (cross-sectional area) of the drogue to all other components. This "drag area ratio" is 40:1 for a GDP drifter (original or "mini"), which results in 0.7 cm s^{-1} of downwind slip in 10 m s^{-1} winds when the drogue is attached (Niiler et al., 1995); for comparison, a standard FGGE-type drifter had a drag area ratio of 10:1–12:1 and a downwind slip of 8 cm s^{-1} in 10 m s^{-1} winds (Niiler and Paduan, 1995; Pazan and Niiler, 2001). Since the collection of Argos fixes is irregular in time and depends on latitude, the drifters' velocity data are interpolated to 6 h intervals with a kriging algorithm (Hansen and Poulain, 1996). The slip of a drogued GDP drifter (original or "mini" version) has not been measured at wind speeds greater than 10 m s^{-1}, but comparisons with altimetric observations suggest that it may exceed 0.07 cm s^{-1} per 1 m s^{-1} wind in these conditions (Niiler et al., 2003b).

When a drifter loses its drogue, the downwind slip increases by ~8 cm s^{-1} per 10 m s^{-1} wind (Pazan and Niiler, 2001), a result that can be exploited to recover low-frequency currents from undrogued drifter data (Pazan and Niiler, 2004). The presence of the drogue was originally detected via a submergence sensor on the surface float of the GDP drifter, as the float is frequently pulled underwater by the drogue. However, this sensor could fail or provide spurious results. In the late 2000s, the submergence sensor was replaced by the more reliable tether strain sensor at the base of the surface float. During the period of faulty submergence sensors in the early to mid-2000s, many undiagnosed drogue losses contaminated the velocity observations of supposedly drogued drifters in the drifter data base (Grodsky et al., 2011), explaining the time-varying behavior of drifter motion noted by Rio et al. (2011a). Subsequently, Rio (2012) developed a method to segregate drogue-off data, although this methodology tended to be overly conservative (i.e., it tended to discard known drogue-on data from some drifters). Lumpkin et al. (2013) adapted Rio's methodology to estimate as closely as possible the date of drogue loss for each drifter in the dataset, and applied this methodology to demonstrate that spurious low-frequency variations in current systems such as the Antarctic Circumpolar Current (ACC) subsequently disappear. Lumpkin et al. (2013) also demonstrated that the existing submergence records could be reinterpreted in a number of cases, and showed that transmission frequency anomalies could also be used to indicate drogue loss. These results have now been exploited in a systematic reevaluation of drogue presence for all drifters in the dataset since October 1992. These multiple criteria (tether strain, anomalous downwind motion, and frequency anomalies) are now used operationally to evaluate drogue presence.

Most of the global array of drifters is managed by the GDP, a component of NOAA's contribution to the Global Ocean Observing System (GOOS) and Global Climate Observing System (GCOS) and a scientific project of the Data Buoy Cooperation Panel (DBCP) of the World Meteorological Organization (Needler et al., 1999). The DBCP constitutes the data buoy component of the Joint WMO-IOC (Intergovernmental Oceanographic Commission) Technical Commission for Oceanography and Marine Meteorology (JCOMM). A full explanation of the structure and operating principles of the DBCP can be found at http://www.jcommops.org/dbcp/. The GDP maintains approximately 90% of the global drifter array, and important contributions are provided by several weather centers by way of barometer upgrades of GDP drifters, purchases of drifters for specific regional programs such as the Surface Marine observation program of the European Meteorological Services Network (E-SURFMAR) and deployment opportunities.

The scientific objectives of the GDP are to provide operational, near-real time surface velocity, sea surface temperature, and sea-level pressure observations for numerical weather forecasting, research, and *in situ* calibration and validation of satellite observations. The GDP is managed in close cooperation between NOAA/AOML in Miami, Florida, SIO in La Jolla, California, and commercial drifter manufacturers. AOML arranges and conducts drifter deployments with numerous national and international partners, processes the data, supervises data quality control, maintains files that describe each drifter, and hosts the GDP website (www.aoml.noaa.gov/phod/dac). SIO supervises the manufacturing industry, acquires most of the drifters, upgrades the technology, and develops new sensors. The GDP is funded by NOAA's Climate Program Office, and has considerable synergy with the Office of Naval Research, which supports instrument development at SIO and the deployment of additional drifters for regional circulation studies (c.f., Sections 4.1–4.4). Drifter data are made available in near-real time on the Global Telecommunications System for weather forecasting efforts, and in delayed mode (approximately three months, after quality control and interpolation) at the GDP web page and (with an additional six months' delay) at the data archive at Canada's Integrated Science Data Management

(ISDM; formerly MEDS), a Responsible National Oceanographic Data Center (RNODC) for drifting buoy data.

The modern dataset of GDP drifters includes all drifters that had a holey-sock drogue centered at 15 m depth, with a drag area ratio of ~40:1. AOML drifters with spar-shaped surface floats and holey-sock drogues were first deployed in February 1979 as part of the TOGA/Equatorial Pacific Ocean Circulation Experiment (EPOCS) (Hansen and Poulain, 1996). Large-scale deployments of the first modern GDP drifters took place in 1988 (WCRP, 1988) in the tropical Pacific Ocean. This effort was expanded to global scale as part of WOCE and the Atlantic Climate Change Program. The first GDP drifter deployments in the tropical Indian Ocean were conducted in 1985, and sustained North Atlantic deployments began in 1989. Sustained South Atlantic deployments began in 1993, at which point the global array had grown to over 500 drifters. Sustained Southern and Indian Ocean deployments began in 1994 (Niiler, 2001), and tropical Atlantic deployments in 1997 (Lumpkin and Garzoli, 2005). In October 1999, when the global array had reached >700 drifters, the OceanObs'99 conference was held to define research and operational oceanography needs, and translate these into goals for various components of the GOOS and GCOS (Needler et al., 1999). The GOOS/GCOS requirement for drifters was determined to be a global array of 1250 drifters at a nominal resolution of 5° × 5°, enough to provide sufficiently dense drifter SST observations to keep the globally averaged maximum potential SST satellite bias error smaller than 0.5 °C (Zhang et al., 2009). In September 2005, the global array reached the goal size of 1250 instruments, and the size of the array has subsequently fluctuated between 875 and ~1350 drifters with an annually averaged size near 1250. The density of quality-controlled observations as of July 2011 is shown in Figure 12.1.

1.2. Mean Surface Circulation

Currently, drifting buoys provide the most reliable measurements of ocean currents at nearly global coverage. Trajectories of even a few drifters can outline the structure of surface circulation in a most graphical manner (McNally et al., 1983). Observations with moored current meters, with ship-borne or lowered acoustic Doppler current profilers (ADCP) or with high-frequency radars (HFR) can provide accurate velocity measurements at particular locations, along lines or near coast lines, but their global distribution is very heterogeneous and these observations will not be addressed in this chapter.

Mean streamlines, computed from the trajectories of nearly 15,000 SVP/GDP drifters, ensemble-averaged in 1/4° bins, shown in Figure 12.2a, delineate the main features of the large-scale surface ocean circulation. These features range from large converging anticyclonic vortices in all five subtropical oceans to narrow jets, some exceeding 1 m s^{-1} in average velocity and 2 m s^{-1} in data of individual drifters. Western boundary currents (WBC) are apparent in Figure 12.2a along eastern shelves of all continents and the dynamics, inducing these currents, is described in Chapter 13 of this book. Chapter 18 addresses the complex system of currents, existing in the Southern Ocean, Chapter 14 describes eastern boundary currents, and Chapter 15 discusses the structure and dynamics of tropical currents.

Perhaps the most striking feature of Figure 12.2a is the complexity of the structure of many frontal zones emerging from the ensemble of high-quality observations, even though these data have been collected quasi-randomly in space and in time. The typical ocean jet is unstable, varying in time, and surrounded by an area of elevated eddy kinetic

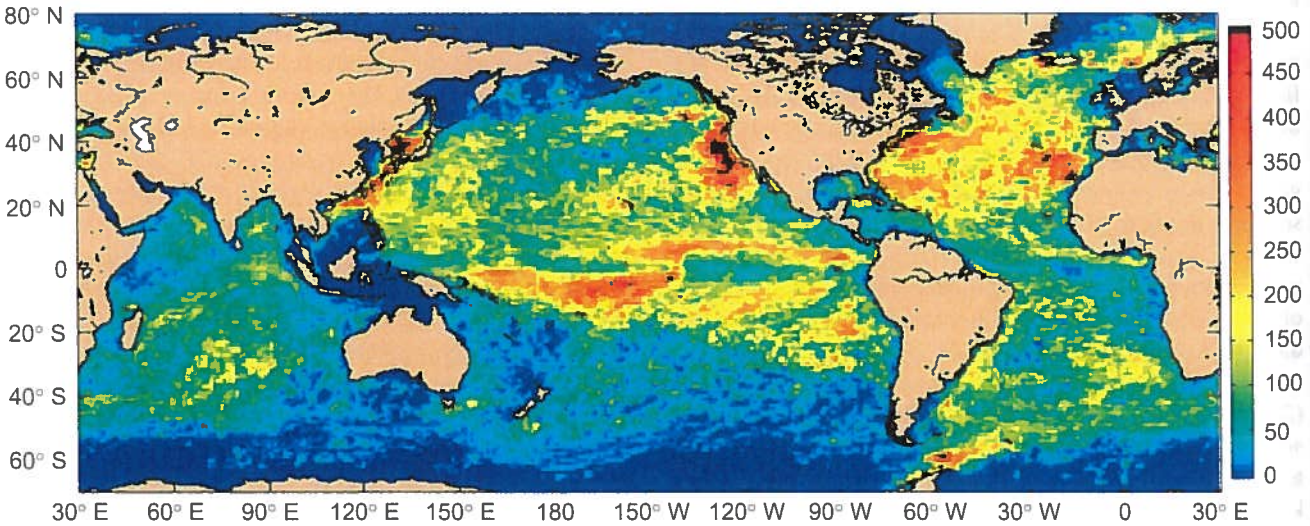

FIGURE 12.1 Density of drifter observations (drifter days per square degree) in the quality-controlled GDP database, with observations spanning the period February 15, 1979–July 1, 2011. Black indicates >500 drifter days per square degree.

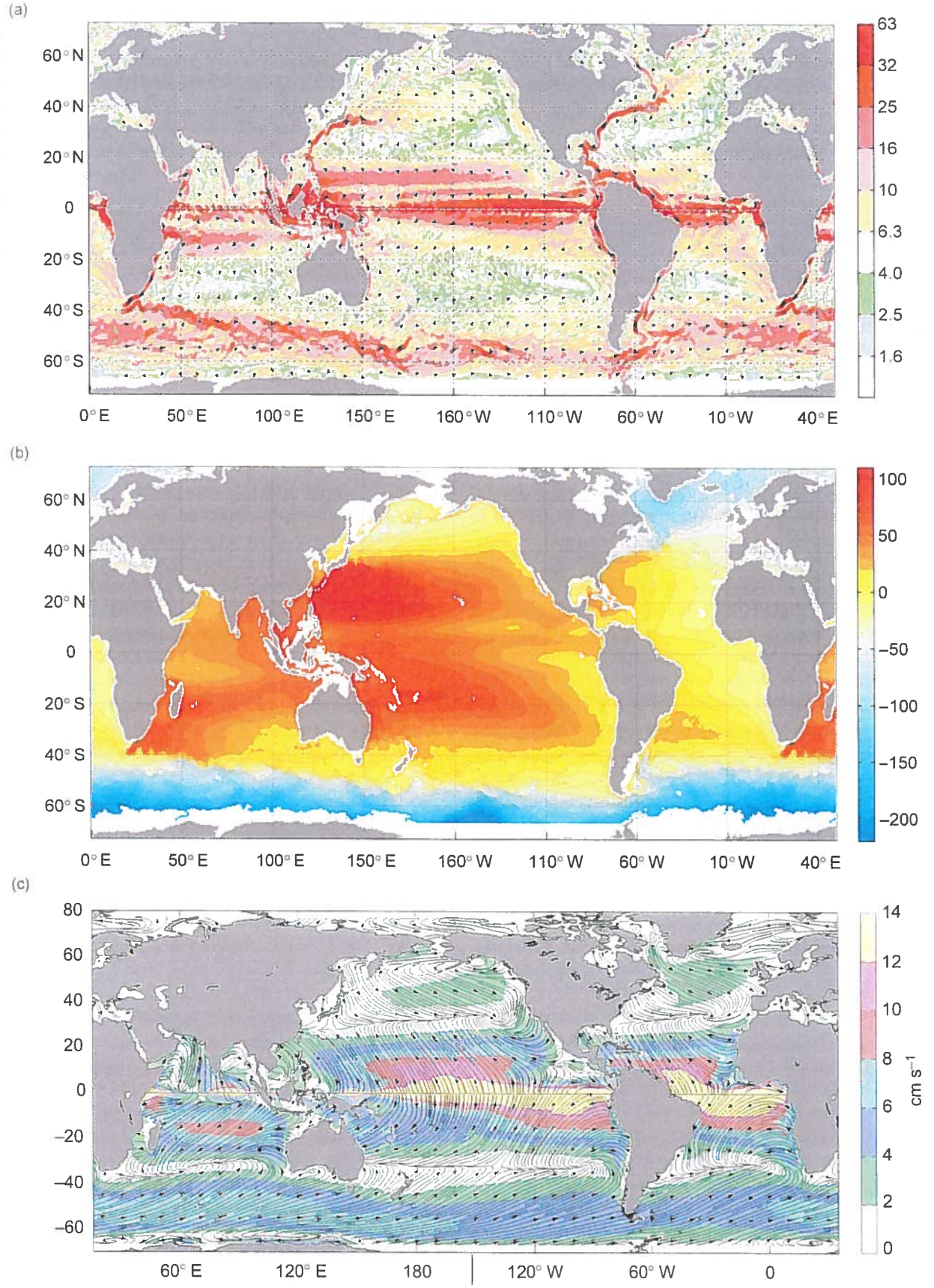

FIGURE 12.2 Ensemble-mean drifter streamlines (a), mean dynamic topography (b), and mean Ekman currents at 15 m depth (c). Units are cm s^{-1} (a and c) and cm (b). *Reproduced from Maximenko et al. (2008).*

energy (EKE) (see Chapter 8). Eddies are known to effectively mix properties of the ocean. One would expect that this mixing (and, correspondingly, averaging data in time) would reduce all contrasts, would broaden fronts and jets, and would eliminate small-scale details from their systems. Yet, many jets remain narrow in the multiyear ensemble average. The Agulhas return current demonstrates as many as seven meanders in the long-time mean (Pazan and Niiler, 2004), while at various times the number of the meanders may vary (Boebel et al., 2003). Centurioni et al. (2008) report four permanent meanders of the California Current, existing despite strong ocean variability in the region. The Kuroshio Extension and Subarctic Front form a system of meandering and branching fronts, visible in time or ensemble averages (e.g., Niiler et al., 2003a). Although the Azores Current exhibits tremendously complex structure on snapshots, its signature in the multiyear average extends all the way across the North Atlantic and nearly reaches the American coast in the west (Klein and Siedler, 1989; Niiler et al., 2003b). Multiple fronts/jets in the ACC, anchored to features on the bottom topography, create tremendously complex flow structure in the Southern Ocean (Hughes, 2005).

The robustness of these mesoscale structures in the time mean can be partly explained by their attachment to bathymetric features. The stability of the extensions may be provided by association of ocean jets with fronts. Baroclinic fronts at the ocean surface are expressions of the three-dimensional interface, separating large water masses. The role of fronts as barriers was studied in the North Pacific by Niiler et al. (2003a) and in the North Atlantic by Brambilla and Talley (2006).

Even the statistics of "perfect" drifters are subject to a number of biases (Davis, 1991), associated with heterogeneous distribution of buoys in space and in time (Figure 12.1). Some heterogeneity results from the deployment scheme of the drifters and induces biases common to all kinds of *in situ* observations (high density of observations in some regions and sparse coverage in other, peak of observations in one season or year followed by background activity at other time periods, etc.). Other biases are essentially due to the Lagrangian nature of drifter observations; in these cases, the sampling scheme is not independent from the sampled velocity field. These effects include dispersion of buoys from areas of high drifter density to areas of lower density, stronger dispersion in the direction of stronger mixing (Freeland et al., 1975), and the effects of surface convergences and divergence that attract or repel drifters from certain areas (e.g., see the pattern of drifter density in the equatorial Pacific in Figure 12.1).

Additional biases may be introduced when Lagrangian and Eulerian statistics are combined. For example, Uchida et al. (1998) found that with a perfect correspondence between drifter- and altimetry-derived velocities collocated along the ASUKA (The Affiliated Surveys of the Kuroshio off Ashizuri–Misaki) line, drifters preferentially sampled locations/periods of larger velocities. As a result, mean drifter currents were up to 30% stronger than the Eulerian mean. Maximenko (2004) showed that this bias appears only in the statistics of Lagrangian particles crossing an Eulerian line (more drifters cross the line when the current is stronger, and no drifter can cross the line at zero velocity) and is eliminated if bin averages are used or data are interpolated onto a space–time Eulerian grid. In some cases, satellite observations, calibrated or referenced using collocated *in situ* measurements, can help to mitigate biases by providing nearly uniform Eulerian datasets in broad space and timescale ranges. Techniques used to assess mean geostrophic and Ekman currents are exemplified in the following sections.

2. GEOSTROPHIC SURFACE CIRCULATION

In most cases advection of properties by ocean currents makes dynamic systems nonlinear and, therefore, complex. However, there are a few regimes in the range of observed ocean parameters which offer simple balances (see Chapter 11). An example of such a regime is geostrophy, in which the Coriolis force acting on a moving water parcel is compensated by the horizontal pressure gradient. For slow, low-frequency currents at the sea surface away from the equator, for which temporal changes, nonlinearity, and viscosity can be neglected, this balance can be simplified to

$$\left(\overline{k}\cdot f\right)\times\overline{V}_g=-g\cdot\nabla h, \qquad (12.1)$$

where $\overline{k}$ is the vertical unit vector, f is the Coriolis parameter, g is the acceleration due to gravity, $\overline{V}_g$ is the geostrophic velocity vector, h is the sea level, and ∇ is the horizontal gradient operator. Equation (12.1) is often used to assess currents using sea level from satellite altimetry or using dynamic topography derived from hydrographic vertical profiles under the assumption that currents become negligibly small at some depth.

2.1. High-Resolution Mean Dynamic Topography

The straightforward way to calculate the mean absolute dynamic ocean topography (MDOT), the signal in sea level due to the ocean circulation, is through determining the deviation of the mean sea surface (MSS), describing the absolute shape of the ocean surface, from the geoid, the equipotential surface defined by rotation and gravity of the earth with its complex distribution of mass. Theoretically, the geoid coincides with the ocean surface in the absence of currents. Both the MSS and the geoid models

have severe limitations. The MSS products are derived by combining many satellite altimetry missions, from repeat-track to geodetic, providing very different horizontal resolution and covering different time periods. On the planetary scale, variations of the geoid due to gravity exceed 150 m, while the range of the sea level due to the ocean dynamics is only about 3 m. The GRACE (Gravity Recovery and Climate Experiment; Tapley et al., 2004) mission has improved the model of the geoid, allowing derivation of the MDOT with 400–500 km resolution. The GOCE (Gravity Field and Steady-State Ocean Circulation Explorer; Johannessen et al., 2003) satellite further advanced the geoid model, allowing MDOT products with 150–250 km resolution (c.f., Le Traon et al., 2001; Rio et al., 2011b; Haines et al., 2011; Knudsen et al., 2011). In addition to accurate measurements of gravity, satellite missions can also measure changes in the gravity field caused by movement of large water masses. These variations are beyond the accuracy of and are not accounted for in the modern MDOT products.

To advance MDOT products to the smaller scales resolved by a constellation of satellite altimeters, a few groups around the world developed techniques that allow assessment of the MDOT based on the synthesis of satellite and *in situ* observations. The idea is largely based on the use of Equation (12.1). The data from an altimeter, flying along repeat tracks, can be freed from the unknown geoid by subtracting the time-mean. The absolute reference for the time-varying part (sea-level anomaly gradient) can then be derived from *in situ* velocity measurements, for example, provided by drifters. Imawaki et al. (2001) successfully applied this technique to study variations of transport of the Kuroshio Current (KC) along the ASUKA line south of Japan.

Two-dimensional velocity maps (Ducet et al., 2000) are computed and distributed by AVISO (Archiving, Validation, and Interpretation of Satellite Oceanographic Data, 1996) as weekly maps on a global 1/3° or 1/4° grid. On large scales, away from strong jets, the biggest error in Equation (12.1) originates from Ekman currents (see Section 3.1). Rio and Hernandez (2003, 2004) removed Ekman currents from drifter velocities using correlations with the local low-frequency wind in 5° boxes. Maximenko et al. (2009) calculated latitude-dependent regression coefficients, using mean NCEP reanalysis wind and the GRACE model of the geoid. In both techniques, coarse-resolution MDOT, derived with help of the geoid model, was refined on mesoscale, using sea-level gradients, estimated from Equation (12.1). To further improve spatial coverage of the *in situ* observations, Rio and Hernandez (2004) added historical hydrographic profiles. Recently, Rio et al. (2011a) updated the Rio'05 MDOT, using accumulated data and a more advanced Ekman model.

The MDOT map of Maximenko et al. (2009) is shown in Figure 12.2b. Major fronts, jets, and currents, described in Section 1.2 are even more sharply delineated in this figure than in the ensemble average of drifter velocities in Figure 12.2a. This is because the "eddy noise," significant in the random ensemble of drifters, has been efficiently suppressed by the technique, using (quasi-) continuous data provided by satellite altimetry.

Outside of strong currents, streamlines of geostrophic velocity differ significantly from streamlines of full (or drifter) velocity. These differences are particularly remarkable in the subtropics and tropics and are defined by the mean Ekman currents, shown in Figure 12.2c. Easterly winds, dominant in the equatorial regions in the Pacific and Atlantic, induce poleward Ekman currents on both sides of the equator. This divergence in the upper ocean is compensated by the upwelling waters fed by the subsurface geostrophic flows, directed toward the equator as seen in Figure 12.2b.

Mean surface circulations in Pacific and Atlantic subtropical gyres provide an excellent illustration of the complex underlying dynamics and kinematics. Convergence of Ekman currents along approximately 30° latitude indicates production by the wind stress of anticyclonic vorticity. According to Sverdrup (1947), the steady state under such forcing can be achieved through the equatorward flow, advecting planetary vorticity (see Chapter 11). Such flows are seen in Figure 12.2b throughout all four subtropical gyres with dynamic topography monotonously increasing from east to west.

2.2. Striated Patterns

Improved MDOT not only allows enhancement of the details of known currents, but also reveals new structures. Figure 12.3, showing the map of zonal geostrophic velocity calculated from such a MDOT and high-pass filtered in two-dimensional (latitude–longitude) space, highlights a web of nearly ubiquitous jet-like features (Maximenko et al., 2008). These features (striations) also exist in long-time ensemble averages of subsurface data of XBT (expendable bathythermograph) and velocities of near-surface drifters. However, in the face of eddy noise that is typically an order of magnitude stronger than striations, the striations are only significant in time averages of quasicontinuous datasets such as satellite altimetry. XBT profiles suggest that the subsurface striations extend to at least 400–800 m depth without noticeable tilt. Numerical models suggest that striations may remain coherent vertically throughout the entire water column (Maximenko et al., 2008).

The dynamics of these striations is not understood yet. Their zonal orientation and characteristics along with their ubiquity lead Nakano and Hasumi (2005), Galperin et al. (2004), and Richards et al. (2006) to conclusions on the relevance of the "Rhines mechanism." This mechanism (Rhines, 1975) is based on the theory of two-dimensional turbulence, whose free development induces zonal jets

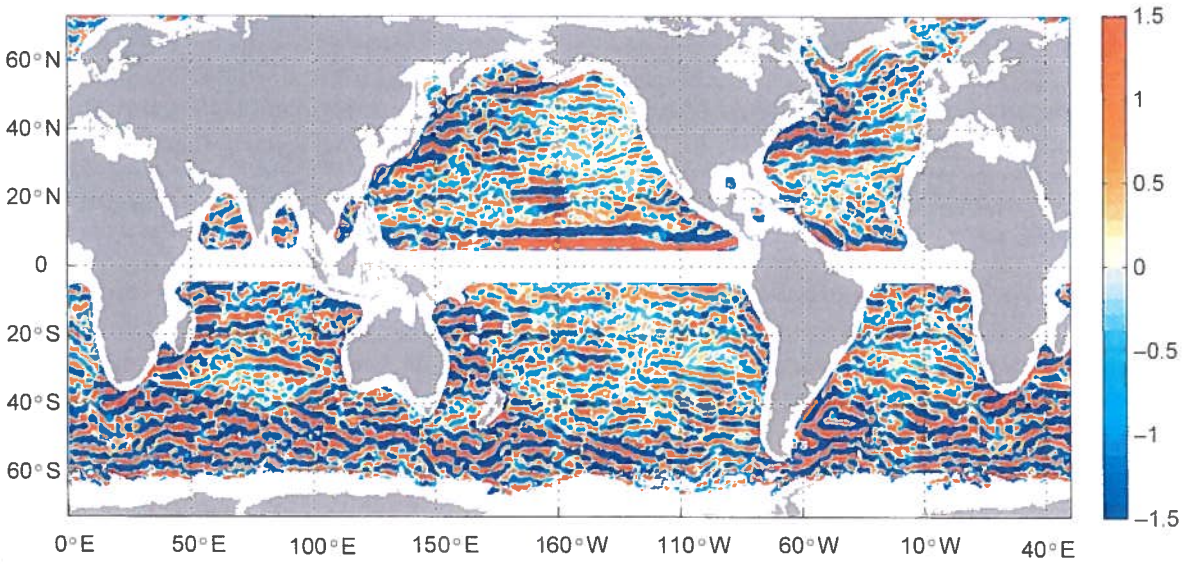

FIGURE 12.3 1993–2002 mean zonal surface geostrophic velocity calculated from the MDOT of Maximenko and Niiler (2005) high-pass filtered with a two-dimensional Hanning filter of 4° half-width. Units are cm s^{-1}. *Reproduced from Maximenko et al. (2008).*

through inverse energy cascade toward larger scales, which becomes limited in the meridional direction on the β-plane by the Rhines scale $L_R = \sqrt{2u'\beta}$, where u' is the r.m.s. eddy velocity and β the meridional gradient of the Coriolis parameter. Baldwin et al. (2007) demonstrated how zonal jets can be generated by breaking Rossby waves, homogenizing potential vorticity within zonal bands.

Careful analysis of the characteristics of time-mean (or stationary) striations reveals deviations from the predictions of these theories. Most importantly, many of these striations do not appear to be inertial jets. This is particularly clear in the eastern parts of subtropical oceans, where mean geostrophic flows are directed toward the equator (Figure 12.2b). When moving across the striations, water parcels only slightly deviate toward the east or west along the axes of striations. In this sense, stationary striations in the east demonstrate properties of waves rather than jets. In addition, these striations appear to be not exactly zonal but have their axes systematically tilted in the zonal direction at angles, consistent with the dynamic of linear Rossby waves trapped at their eastern edges.

Such dynamics can be described as the β-plume (Pedlosky, 1996), generated by a local source of vorticity. Classical β-plumes form a set of nearly zonal currents and extend infinitely to the west from the forcing areas. β-plume dynamics have been suggested to be responsible for the formation of the Azores Current (Kida et al., 2007) and the Hawaiian Lee Countercurrent (Xie et al., 2001). Recently, Centurioni et al. (2008) have found the link between the striated pattern of zonal current velocity off the California coast and areas of upwelling and downwelling, induced by nonlinear interaction of wind-forced Ekman currents and permanent meanders of the California Current. In support of the β-plume mechanism, analysis of striations in Figure 12.3 shows that many of them have at their eastern tips features (such as an island or sea mount or cape in the coast line, etc.) that may anchor vorticity production by wind stress curl or through a more complex dynamical process.

While averaging data in time to suppress the noise from eddies is important (Huang et al., 2007), the very same averaging may produce artificial striations by smearing moving eddies (Schlax and Chelton, 2008; Scott et al., 2008). Huang et al. (2007) and Scott et al. (2008) show that without applying time averaging, the anisotropy of velocity data is very low and increases with the increase of the averaging period. Schlax and Chelton (2008) used a simple statistical model to demonstrate that the signal from the strongest eddies may remain significant even in very long time averages. At the same time, Scott et al. (2008) showed that the distribution of eddies in space is not random and that in some regions the eddies are moving along preferred paths. Although not included into the model of Schlax and Chelton (2008), this heterogeneity is seen in eddy trajectories, shown in their Figure 1.

Buckingham and Cornillon (2013) used data of Chelton et al. (2011) to isolate contribution of eddies to striations. They showed that time-averaged signal from correctly positioned eddies correlates highly with striations in MDOT. At the same time, they found that, contrary to Schlax and Chelton (2008), contributions from moderate-amplitude eddies is important and amplitudes of striations significantly exceed expectations from eddies.

Maximenko et al. (2005) discussed the role of time averaging for a different kind of striation—quasizonal jet-like features seen in the satellite sea-level anomaly as crests and troughs propagating in the subtropical latitudes toward the equator. They showed that eddy "streaks" in time averages, corresponding to the distances traveled by

individual eddies during the average time, are significantly shorter than the length of the striations. In a wide range of periods, individual streaks interact without canceling each other; this is only possible if eddies of the same sense of rotation are aligned along the axes of striations.

The mechanisms that set these alignments or preferred areas of eddy formation or preferred paths of their propagation are not understood yet, but they point to the existence of higher organization of the eddy field than suggested by today's theory. While eddy terms in the vorticity balance of stationary striations are significant, their contribution to the balance differs between the striations (Melnichenko et al., 2010). Striations, having thermal signature at the sea surface, seem to be able to sustain their structure through the locally induced wind stress (Sasaki and Nonaka, 2006). A number of groups are currently working to understand the correspondence between the striated patterns of ocean currents, linear waves, nonlinear eddies, instability of the large-scale flow, and various kinds of external forcing.

2.3. Variability and Trends

EKE derived from AVISO geostrophic currents and from drifter observations is shown in Figure 1 of Chapter 8. For the drifter observations, only drogued drifters were used; velocities were first low-pass filtered at 5 days to remove tides and inertial oscillations, then the time-mean currents—calculated in 1° bins—were removed. As noted by previous researchers (Fratantoni, 2001), the drifter observations have higher EKE throughout most of the world oceans, due to the presence of ageostrophic motion (see Section 3) and geostrophic motion not resolved in the smoothed AVISO fields.

Long-term variations in surface EKE have been observed in a number of regions. A southward shift in the position of the Gulf Stream extension has been inferred from altimeter-derived EKE for the period 1993–2008 (Lumpkin et al., 2009). The Kuroshio Extension has been observed to vary in its stability on decadal timescales, transitioning from a relatively stable phase with lower EKE to an unstable phase with higher EKE, an oscillation perhaps driven by the Pacific Decadal Oscillation (Qiu and Chen, 2005). Over the time period 1993–2000, the confluence of the Brazil and Malvinas Currents in the southwest Atlantic Ocean shifted southward (Lumpkin and Garzoli, 2010), with a corresponding shift in the EKE maximum of the confluence front. This trend may have been part of a multidecadal oscillation forced by SST anomalies imported from the Indian Ocean along the Agulhas–Benguela pathway (Lumpkin and Garzoli, 2010).

The spatial pattern of the trend in the sea-level rise, observed by satellite altimeters between 1993 and 2009 (Willis et al., 2010), has a complex structure and reflects low-frequency changes in surface circulation. More on seasonal and interannual variability can be found in Chapter 24 and decadal variations in Chapter 25.

3. AGEOSTROPHIC CURRENTS

While geostrophy, discussed in the previous section, offers a simplified description of an important class of currents, most of the processes responsible for generation, equilibration, and damping of the currents are more complex. The following subsections will discuss important examples of ageostrophic currents.

3.1. Motion Driven by Wind

The most energetic ageostrophic currents near the ocean surface are directly wind driven. The frequency of the ocean surface's inertial (resonant) response to large-scale wind variations is set by the Coriolis effect, with potential modification by the background vorticity (Kunze, 1985). The resulting near-inertial oscillations are a prominent feature of Eulerian (c.f., Alford and Whitmont, 2007) and Lagrangian (c.f., Elipot and Lumpkin, 2008) spectra, and may represent a significant portion of the energy input needed to maintain the abyssal stratification via interior diapycnal mixing (Munk and Wunsch, 1998). The distribution of near-inertial variance in the mixed layer has been mapped globally using surface drifter observations (Chaigneau et al., 2008); compared to the planetary vorticity set by the Coriolis parameter f, the peak frequency of near-inertial oscillations is blue-shifted equatorward of 30° N/S latitude and is demonstrably affected by the background geostrophic vorticity (Elipot et al., 2010). It is uncertain how much of this energy leaves the upper ocean in trapping regions (c.f., Polzin, 2008) to propagate into the ocean interior.

At lower frequencies, the ocean response to wind forcing was first described by Ekman (1905). With the assumption of a constant diffusivity in an upper boundary layer, Ekman showed that this response was 45° to the right (left) of the wind at the surface in the northern (southern) hemisphere, with the exponentially decaying currents rotating further to the right (left) with increasing depth within the turbulent boundary layer, and a net transport at 90° to the right (left) of the wind. Subsequent research has questioned the assumption of a constant diffusivity and the resulting specific details of the Ekman spiral, although some observations are quantitatively consistent with Ekman's spiral and net transport (c.f., Chereskin, 1995). Using 1503 drogued GDP drifter observations in the period 1988–1996, Ralph and Niiler (1999) demonstrated the validity of Ekman theory across the tropical Pacific basin. Ralph and Niiler (1999) first removed time-mean geostrophic currents using hydrography-based climatologies, along with the wind-driven downwind slip (0.07 cm s^{-1} per 1 m s^{-1} wind; Niiler et al., 1995), and low-pass filtered the residual drifter currents at 5 days to remove near-inertial oscillations and high-frequency tides. They then considered a number of models for regressing the residuals onto the winds in 2° (meridional) by 5° (zonal) bins. They found that the best-fit model was close to $u_{Ek} = Au_*/\sqrt{|f|}$, where u_{Ek} is the

magnitude of the Ekman current, $u_* = \sqrt{\tau/\rho}$ is the friction velocity due to the surface wind stress τ, ρ is the water density, and the best-fit coefficient $A = 0.065 \pm 0.002\ s^{-0.5}$. The Ekman current was directed to the right (left) of the wind in the northern (southern) hemisphere, with an off-wind angle varying according to the ratio of the drogue depth to the Ekman scale depth $H_* \propto u_*/\sqrt{|f|}$ in a manner consistent with a rotating Ekman spiral (Figure 5 of Ralph and Niiler (1999); Figure 4.1.9 of Niiler (2001)). Niiler (2001) updated this study using drifter data through 1999, and found a similar result with $A = 0.081 \pm 0.013\ s^{-0.5}$ for NCEP reanalysis winds.

Rio and Hernandez (2004) expanded upon Ralph and Niiler's (1999) study by removing the time-varying geostrophic motion using altimetry. Rio and Hernandez (2004) modeled the Ekman response as $\overline{u}_{Ek} = b\,\overline{\tau}\,\exp(i\theta)/\sqrt{|f|}$ (i.e., proportional to wind stress, not wind speed as in Ralph and Niiler, 1999) and allowed the coefficients b and angle off the wind θ to vary spatially and seasonally on a 5° grid. They found the angle θ varied in a manner consistent with spatial and seasonal changes in upper-ocean stratification and consequent stretching/compressing of the Ekman spiral compared to the 15 m drogue depth of the drifters. An update of this Ekman parameterization was used to derive the 2009 CLS mean dynamic topography (Rio et al., 2011a). Figure 12.2c shows the mean streamlines of Ekman currents computed using the NCEP reanalysis wind and data from drifters, altimetry, and GRACE.

Although drifter slip has been measured at wind speeds up to 8 m s^{-1}, little is known of their water-following characteristics at higher wind speeds (Niiler et al., 2003a). Wind models with spatially varying coefficients, such as that of Rio and Hernandez (2004), indicate a larger downwind motion at higher latitudes than suggested by the Ralph and Niiler (1999) model with its constant coefficient. This may indicate enhanced downwind slip at high wind and wave states. A number of candidates could account for this: it is possible that wave-driven Stokes drift is generating significant downwind motion in the extreme wave states found, for example, in the ACC (Niiler et al., 2003b). Alternatively, the drifters may be trapped in Langmuir jets at the convergence of the wind- and wave-driven cells (c.f., Thorpe, 2005), and thus not exhibiting slip with respect to currents at 15 m but rather biased sampling compared to an Eulerian average. It is also possible that in extreme wave states the drogue is jerked upward such that its mean depth is significantly above 15 m. Direct measurements of pressure and currents at the top and bottom of the drogue are obviously needed in these conditions to better understand the measurements.

3.2. Centrifugal Effects

Eddy kinetic energy from altimetry is often compared to that from drifters, with the difference attributed to wind-driven motion and smaller scales not resolved by altimetry. Another source of discrepancy, when altimetric currents are derived from pure geostrophy, is the centrifugal effect of the nonlinear term in the momentum equation. This can play a nonzero role in the mean momentum budget in a region if vortices of one sign dominate, for example the cyclonic cold-core rings south of the mean Gulf Stream jet. To see the effect of this term, consider an azimuthally-symmetric vortex governed by the momentum equation

$$v^2/r + fv = g\partial_r \eta, \tag{12.2}$$

where r is the distance from the center of the vortex, v the speed of the vortex, g is gravity, f the Coriolis parameter, η is sea surface height, and $\partial_r \eta$ is its derivative along r. Suppose altimetry gives $\eta = fa(r^2 - R^2)/2g$ to radius R and $\eta = 0$ for $r > R$, with a constant, and geostrophy is assumed (the first term in the momentum equation is dropped). Then $v_{geo} = ar$ within the solid-body vortex. However, when the centrifugal term is included, a Taylor series expansion for small Rossby number a/f gives $v = ar(1 - a/f + \ldots)$. For a cyclonic vortex ($a/f > 0$), the actual velocity is less than the estimate from pure geostrophy; for an anticyclonic vortex, the magnitude of the velocity is higher. For the Kuroshio south of Japan, Uchida et al. (1998) showed that centrifugal effects due to the curvature of the current axis explain well the 10% difference between drifter and geostrophic velocities.

Fratantoni (2001) compared EKE from altimeter-derived geostrophic velocities and from 2-day low-passed drifter velocities in the North Atlantic basin, and found that drifter EKE was generally higher by O(100 $cm^2\ s^{-2}$). He attributed this to the directly wind-forced motion in the drifter velocities. However, he found a fascinating pattern in the drifter minus altimeter EKE (his Plate 8) in the immediate region of the Gulf Stream front: altimeter EKE exceeded drifter EKE by >250 $cm^2\ s^{-2}$ immediately south of the mean Gulf Stream extension, while the opposite was true immediately to the north. Fratantoni (2001) attributed this to differences in the Gulf Stream location in the two datasets due to differences in resolution and smoothing between the data. However, this pattern is exactly what one would expect if the centrifugal term is playing a significant role in the surface momentum budget, as noted by Niiler (2003a) who found that the centrifugal term can alter the magnitude of currents on either side of the Kuroshio jet by as much as 25%. Consistent with this interpretation, Niiler (2003a) found maximum values of altimeter-derived geostrophic EKE in the Kuroshio extension region shifted south of the maximum indicated by drifters (their Figure 7). Maximenko and Niiler (2006) mapped dominant eddies using the skewness of the probability density function of sea-level anomaly $\langle h'^3 \rangle / \langle h'^2 \rangle^{3/2}$, derived from satellite altimetry, and energy-weighted angular velocity $\omega_E = \left\langle \overline{V} \times d\,\overline{V}/dt \right\rangle / \left\langle \overline{V}^2 \right\rangle$, computed from drifter trajectories. The two maps demonstrate remarkable resemblance and reflect the prevalence of anticyclonic eddies north of the Gulf Stream and cyclones on the southern side.

3.3. Nonlinear Interactions with Baroclinic Features

The ageostrophic component of ocean currents also plays a major role in the three-dimensional upper-ocean circulation, for which much of our knowledge derives from theoretical and idealized, process-modeling, numerical studies.

The secondary circulation created by a wind blowing parallel over a geostrophically balanced current was studied by Lee et al. (1994) who concluded that, after the near-inertial fluctuations dissipate, the Ekman vertical velocity is enhanced by the horizontal shear of a geostrophic flow when a nonlinear model is used. In this case, a downwelling/upwelling pattern emerges in the mixed layer. For a wind blowing in the direction of the current, the upwelling area is narrow and confined in the region of positive relative vorticity and the downwelling region is broad and on the side of negative relative vorticity patch. The situation is reversed if the wind and the jet flow in opposite directions. While this mechanism could potentially play a role in determining the magnitude of the vertical fluxes of heat, momentum, and nutrients, the observational evidence is still scant.

When a wind stress is applied to a subtropical anticyclonic eddy (Lee and Niiler, 1998), cold water is advected over warm water, which induces vertical mixing and downwelling. A nonlinear numerical model solution shows that a downwelling region results, which is larger and more intense than the upwelling area located on the opposite side of the eddy. The residual secondary circulation induced by the nonlinear interaction between the wind-induced Ekman flow and the eddy resembles a jet that cuts across the eddy core. The ageostrophic velocity computed from a Regional Ocean Modeling System (ROMS) simulation of the California Current System (CCS) (Marchesiello et al., 2003) shows a pattern that is consistent with the effect described by Lee and Niiler (1998) when a wind parallel to the coast is blown over the permanent meanders of the CCS (Centurioni et al., 2008), which are essentially a series of alternating cyclonic and anticyclonic mesoscale features.

4. REGIONAL SURFACE OCEAN DYNAMICS

The true complexity of the dynamics of surface currents can be illustrated through more careful look at particular regions, highlighted in the following sections.

4.1. Drifter Studies in the California Current System

The CCS is a broad and generally southward eastern boundary current of the subtropical North Pacific (Chapter 14). Upwelling in the CCS region occurs in summer (i.e., when northwesterly winds occur) between 35° N–38° N and 46° N, and downwelling primarily occurs in winter in the same region (i.e., when the winds shift to the SE). South of 35° N–38° N upwelling occurs throughout the year (Huyer, 1983). In the past four decades, Lagrangian drifters were used extensively to map the structure of the surface circulation of the CCS and of the near-shore surface flow. Investigations of the CCS with Lagrangian drifters include regional studies (e.g., McNally et al., 1983; Davis, 1985b; Poulain and Niiler, 1989; Swenson et al., 1992; Swenson and Niiler, 1996; Winant et al., 1999; Austin and Barth, 2002) as well as studies leveraging on the large historical dataset accumulated through nearly three decades of deployments (Centurioni et al., 2008) of GDP drifters (Niiler, 2001).

The drifter-derived, 15-m deep geostrophic velocity is often approximated by subtracting the Ekman velocity (e.g., Ralph and Niiler, 1999; Centurioni et al., 2009) from the measured drifter velocity. Such an approximation holds for most large-scale flows, including when currents are not in cyclostrophic balance (Equation 12.2), when the flow is weakly nonlinear, when drifters are not inside Langmuir cells and when the Stokes' drift is not a significant fraction of the total velocity. Additionally, the tidal and near-inertial components of the flow are filtered out along the drifter track. Because of their characteristic space and timescales, the ageostrophic, non-Ekman currents, are in most cases filtered out by averaging all of the available observations within rather large spatial bins. An interesting aspect of the CCS is that the vector correlation between the drifter-derived geostrophic velocity residual, computed with respect to the mean, and the corresponding quantity obtained from satellite altimetry data is large offshore of the US west coast (>0.8) and drops to low or negative values in a near-shore strip about 200 km wide, suggesting that the near-shore flow is either nongeostrophic or has time and spatial scales, which are not adequately resolved by the weekly, 1/3°, satellite altimetry maps (Centurioni et al., 2008). Vigorous highly nonlinear eddies 600–800 m deep (Chereskin et al., 2000) as well as cold water filaments (Strub et al., 1991) have been observed in the upwelling regions of the US west coast and the timescales of those coherent structure range from 2 to 7 days near the coast (Swenson et al., 1992; Chereskin et al., 2000), and are of the order of 30 days and longer as the eddies move further offshore (Swenson et al., 1992).

The combined analysis of SVP/GDP drifter and satellite altimetry data has revealed the existence of at least four permanent meanders of the CCS, which are connected to a set of slanted bands of primarily eastward zonal flow (Figure 12.4; see also Centurioni et al., 2008). The spatial structure of the CCS meanders is seasonal (Figure 12.5), with the strongest near-surface currents observed in summer (JAS) and the most pronounced meanders occurring in fall (OND).

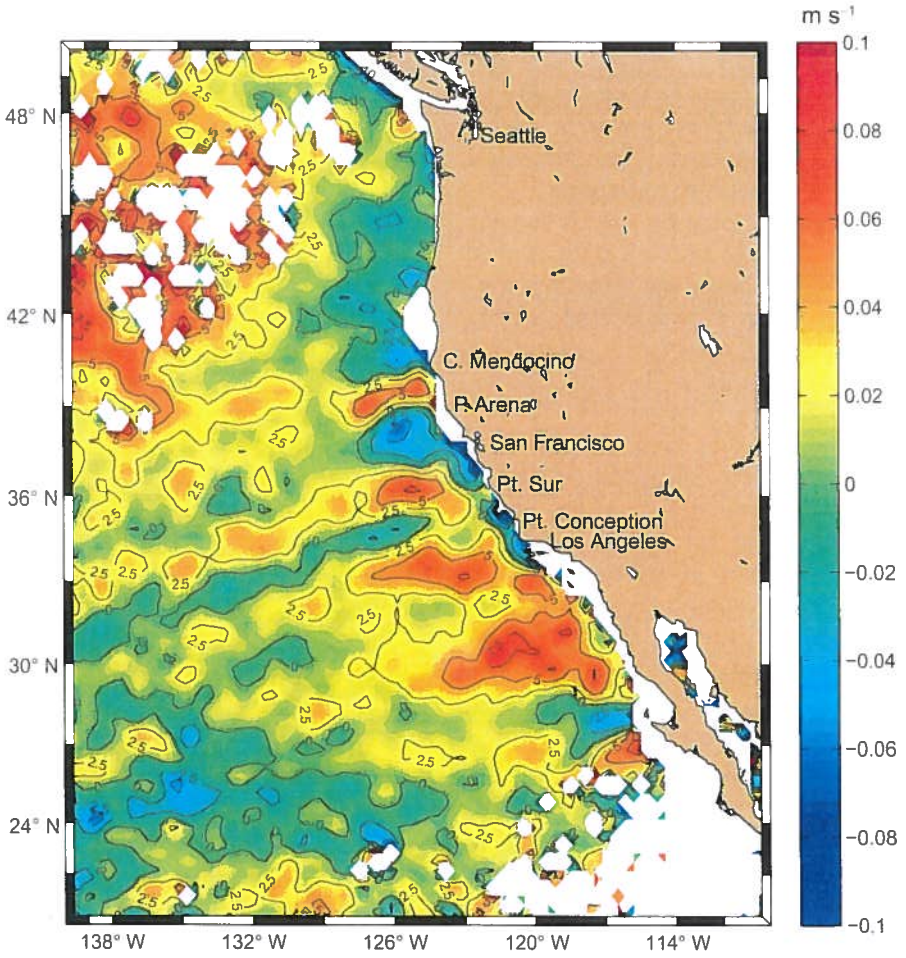

FIGURE 12.4 Near-surface unbiased geostrophic zonal flow in the eastern North Pacific. Year-long ensemble-average between July 1992 and June 2011. Note the four bands of eastward velocity whose easternmost expression is colocated with the CCS meanders. Refer to Centurioni et al. (2008) for the methodology used to compute the velocity field.

An interesting scientific question is which physical processes are responsible for the meandering structure of the CCS system. The acceleration of the near-surface water particles computed from drogued drifters is significantly larger in the near-shore strip and where the meanders occur than further offshore in the proximity of the "eddy desert" region (Cornuelle et al., 2000). The implication of this finding is that the departure from a pure geostrophic balance is larger in the CCS meanders than elsewhere. Eddy and mean vorticity fluxes are likely to act as one of the forcing mechanisms that dictate the shape of the CCS (Centurioni et al., 2008).

Direct velocity observations from Lagrangian GDP drifters are therefore particularly important in regions where the departure from geostrophy is largest or where the time and space scales of the flow are not adequately sampled by the ongoing satellite altimetry missions. The residence time of the drifters in the CCS is short especially near the coast because the surface flow there is highly divergent. Long-term and sustainable deployment programs are therefore important to further our understanding of the dynamics of the near-shore part of the CCS.

4.2. Drifter Studies off Senegal

Another surface divergent region where drifters' deployments have begun in recent years is the tropical North Atlantic off Senegal (Chapter 14). The Senegalese coast has perhaps the largest seasonal and interannual variation of oceanographic conditions of the entire west coast of Africa. It is also the African coastal region where the Pacific El Niño's influence is felt the strongest (Bhatt, 1989; Roy and Reason, 2001). On a seasonal and interannual basis, the surface waters from the equatorial region moving northward are separated by a strong frontal region perpendicular to the coast from the waters with origins in the subtropical gyre (Wooster et al., 1976) that move generally southward (Lumpkin and Garzoli, 2005). This frontal region moves south to north along the Senegal coast on both seasonal and interannual timescales (Wooster et al., 1976).

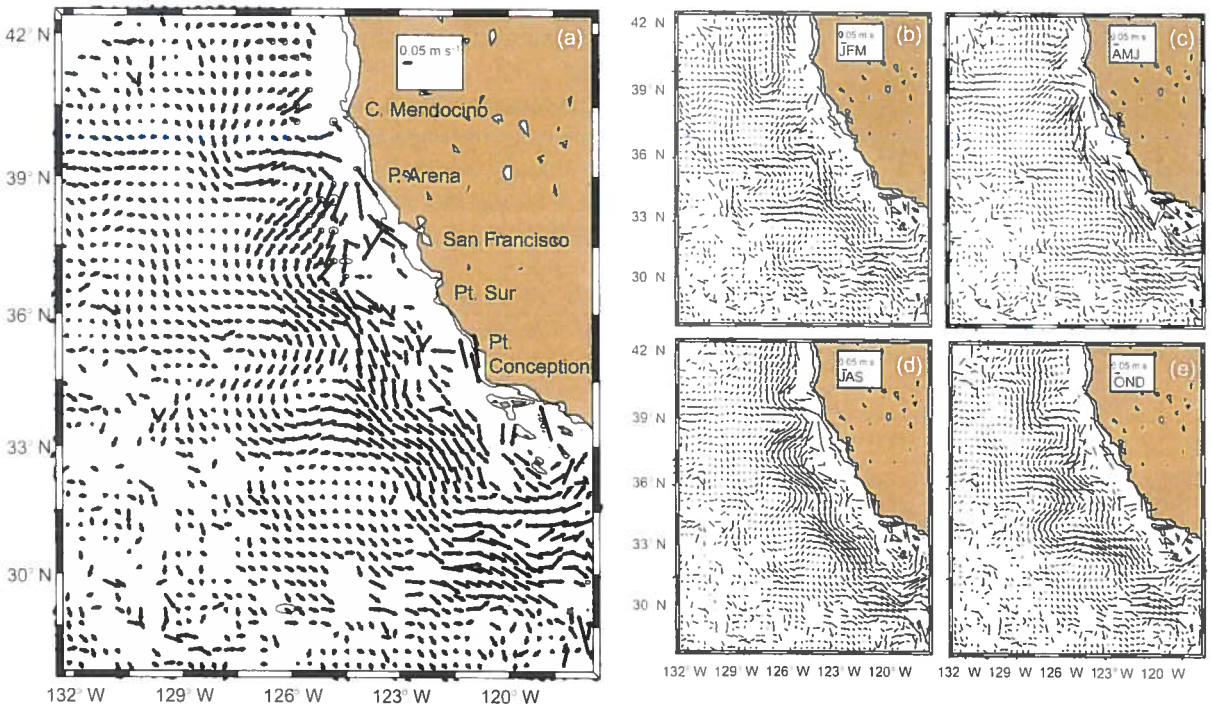

FIGURE 12.5 Near-surface unbiased geostrophic velocity field in the California Current System. Year-long (a) and seasonal (b–e) ensemble-average between July 1992 and June 2011. Note the increase of the intensity of the currents in summer (JAS) and the larger extent of the meanders in fall (OND).

Time-averaged confluence front can be seen in Figure 12.2a around 15–20°N. Although the drifter observations are sparser in this area than in any other part of the North Atlantic (Figure 12.1), a time-mean geostrophic, near-surface flow to the north, is indicated to exist by the data (Figure 12.2a).

The strongest upwelling system appears to be associated with the southward wind-driven circulation that is set up north of Cape Verde during La Niña years, generally in the early spring season (Roy and Reason, 2001). Under these conditions, a strong jet of upwelled water flows southward and leaves the coast at the tip of Cape Verde, and appears to set up a quasi-zonal frontal system nearly 10° of longitude into the eastern North Atlantic (Wooster et al., 1976). The flow patterns off the coast of Senegal express both upwelling and downwelling conditions and are further complicated by seasonal fresh water inflow from the Senegal, Gambia, and Casamance rivers (Bhatt, 1989).

Lagrangian GDP drifters are currently being used to improve the description of the near-surface circulation off the coast of Senegal. Lagrangian methods, when joined together with satellite data, are very powerful in determining the patterns of flow, especially when repeated over several years and seasons. But these data can be very misleading when small numbers over short timescales are used to make inferences. The emerging picture from more than two years of targeted drifter deployment off Senegal is that of a year-round, offshore directed near-surface flow north of Cap Vert peninsula, the westernmost point of Africa. In the ongoing project, the time-dependent sketches obtained by combining the unbiased geostrophic velocity field derived with the technique of Centurioni et al. (2008), the time-dependent, altimetry-derived geostrophic currents, and the Ekman flow were computed at weekly intervals and have confirmed the existence of broad filaments of intense (in excess of 15–20 cm s^{-1}) currents and rings off the coast of Senegal.

4.3. Interaction of the Kuroshio with the South China Sea

The KC, a major WBC of the North Pacific (Chapter 13), is about 140 km wide east of the islands of Luzon and Taiwan (Figure 12.6) and flows essentially northeastward with a speed of 1–1.5 m s^{-1} (Centurioni et al., 2009). The Kuroshio emerges out of a region dominated by eddy-like flow just north of where the North Equatorial Current ends in the proximity of the Philippines coast (Centurioni et al., 2004; Rudnick et al., 2011). The volume transport of the KC is between 23 and 32 Sv (1 Sv = 10^6 $m^3 s^{-1}$) at 18.5° N (Yaremchuk and Qu, 2004) and averages 21.5 Sv through the East Taiwan Channel (Johns et al., 2001). Part of the KC seems to recirculate southward east of the Ilan Ridge and northeastward east of the Ryukyu Islands (Nitani, 1972), as also suggested by the synthesis of drifter and satellite altimetry data (Imawaki et al., 2003).

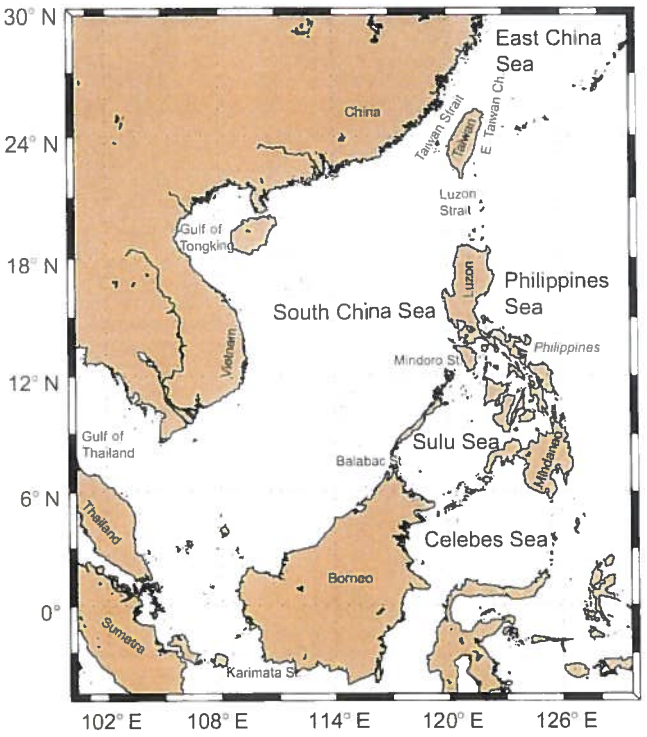

FIGURE 12.6 Map of marginal seas in the southwestern part of the North Pacific. Interaction of the Kuroshio with the South China Sea is described in Section 4.3 and with the East China Sea in Section 4.4.

The interaction of the KC with the South China Sea (SCS, Figure 12.6) occurs primarily through the Luzon Strait (LS), which has a sill depth generally above 2400 m and a bathymetry complicated by numerous islands and channels. The KC usually flows straight north across the LS, but occasionally it intrudes into the SCS, sometimes forming a loop current (Hu et al., 2000). A somewhat similar phenomenon occurs in the Gulf of Mexico where the Gulf Stream leaps from Yucatan to Florida but occasionally intrudes as a deeply penetrating loop current that sheds eddies into the Gulf of Mexico (Hofmann and Worley, 1986; Romanou et al., 2004).

Direct velocity observations from SVP/GDP drifters between November 1986 and May 2002 have provided further evidence of the occurrence of Philippine Sea water (PSW) intrusions into the interior of the SCS between October and January (Centurioni et al., 2004, 2009), with 15-m depth westward currents of the order of 1 m s^{-1} within the LS. Such strong current cannot be solely explained by Ekman currents generated by the northeast monsoon. The 15-m depth Ekman velocity that would be produced by monsoon winds is at most 0.25 m s^{-1} (Centurioni et al., 2009), and the stronger surface currents observed by the drifters indicate that a deeper current system to the west must be present (Centurioni et al., 2004, 2009). The associated westward Ekman transport through the LS computed from satellite Special Sensor Microwave Imager (SSM/I) winds reaches a maximum of 0.6 Sv in December (Centurioni et al., 2004). Drifter velocity data also confirm the existence of a fall through winter anticyclonic circulation (loop) southwest of Taiwan (Centurioni et al., 2004), agreeing with previous hydrographic observations (Nitani, 1972).

Many of the drifters that enter the SCS through the LS during the northeast monsoon do not move back to the Philippine Sea (PS) within the KC loop, but move rapidly into a current along the western margin of the deep SCS basin and continue to travel southward along the coast of Vietnam, with speeds in excess of 1 m s^{-1} (Hu et al., 2000; Centurioni et al., 2004, 2009). During the Asian southwest monsoon, which occurs in boreal spring and summer months, drifters deployed in the SCS have shown that the exchange of surface water between the SCS and the PS is reversed, with drifters now exiting the SCS through the LS and the Taiwan Strait (Centurioni et al., 2007).

The swift jet off Vietnam, whose surface signature is clearly revealed by the drifters, is mainly concentrated inshore of the 200 m isobaths and has speeds two to three times larger than previous estimates (Liu et al., 2004). The downwelling region offshore of Vietnam that stretches parallel to the coast is probably responsible for maintaining the pressure gradient balanced by the Coriolis force acting on the southward flowing jet (Gill, 1982). New subsurface observations are needed there to elucidate the vertical structure of this boundary current. At about 11° N, offshore southeast Vietnam, the current veers onto the continental shelf probably as a consequence of the approximately westward Ekman transport that develops during the northeast monsoon and associated downwelling and an extended region of Ekman pumping (Liu et al., 2004; Centurioni et al., 2009). Because of the strong northeasterly monsoon wind blowing in the direction of the sheared jet, a relatively strong secondary circulation with upwelling concentrated to the east and southeast of the jet should arise (Lee et al., 1994), thus enhancing the slopes of the isopycnals that maintain the dynamical balance of this current system (see also Section 3.3).

The results mentioned earlier strongly suggest that a net westward volume transport of PSW into the SCS occurs through the LS in the top few hundred meters between October and January. One interesting and still unanswered scientific question is where does the compensating SCS outflow occur? All the other straits that connect the SCS with the adjacent basins from which the fall/winter PSW inflow could be balanced by outflow are much shallower than the LS: the Taiwan Strait is on average 60 m deep, the Malacca, Gaspar and Karimata Straits have sills shallower than 50 m, and the Balabac and the Mindoro Straits connect the SCS to the Sulu Sea with passages that are about 100 and 450 m deep, respectively. It is still unclear how the volume balance of the SCS can be closed only by way of outflow from shallow passages (or deep and narrow in the case of the Mindoro Strait). Qu (2000) used

hydrographic data to compute a geostrophic volume transport from 0 to 400 m of 5.3 Sv westward in January through February. Drifter releases in the north SCS suggest the existence of a current system that connects the LS region with the southwest equatorial SCS. A 5 Sv outflow from the SCS through the Karimata Strait (approximately 200 km wide and 30 m deep) would require a persistent average current through fall and winter of 0.8 m s^{-1}. It is not known whether or not such flow exists. Outflow from the SCS could also occur through the LS below the inflowing PSW layer, which requires water mass conversion that transforms the warm and salty PSW surface water into the cooler and fresher SCS deeper water. The concept of SCS water outflow below the PSW layer from the LS is not new since SCS waters characterized by a salinity minimum in the potential density/salinity space, which are normally found between 350 and 1350 m depth (Chen and Huang, 1996), were tracked as far north as Japan and are thought to have escaped through the LS (Chen, 2005). Furthermore, using the distribution of dissolved oxygen, Li and Qu (2006) showed the evidence for a sandwiched vertical structure in transports through the LS, with outflows in the intermediate layer (700–1500 m) and inflows above and below.

Quantifying the net inflow of PS/KC water into the SCS is an important step to better document the meridional heat fluxes in the north Pacific. New drifter deployments in the southern SCS will provide useful data to better understand the structure of the SCS near-surface circulation and therefore to address some of the science questions mentioned earlier.

4.4. Interaction of the Kuroshio with the East China Sea

The KC is known to interact with the East China Sea (ECS, Figure 12.6) by way of intrusions of the latter on the continental shelf northeast of Taiwan (Gawarkiewicz et al., 2011). SVP/GDP drifters from the historical data archive together with repeat releases designed to map the intrusion events suggest that deep excursions of the KC on the ECS continental shelf have a meandering nature and occur all year round, perhaps with a weak seasonal modulation (Vélez-Belchí et al., 2013).

The dynamics of the intrusion is still unclear, but there is evidence of a link between cyclonic mesoscale eddies coalescing with, or being advected by the KC east of Taiwan, low transport of the KC through the East Taiwan Channel, and ECS shelf intrusions of the KC (Vélez-Belchí et al., 2013). The time variations of the northward transport of the KC through the East Taiwan Channel on the I-Lan Ridge were measured with an intensive current array PCM-1 during WOCE (Johns et al., 2001). Remarkably, this transport varies with a period near 100 days, and no significant seasonal cycle was detected by these direct measurements. The variations of this transport are correlated with the presence of mesoscale eddies directly east of Taiwan in the northern PS (Zhang et al., 2001). A presence of a cyclonic eddy is accompanied with low KC transport and anticyclonic eddy with a high KC transport. The correlation between the WOCE PCM-1 KC transport and the AVISO gridded weekly sea level anomaly (SLA) data is maximum (0.83) at 23.9° N, 123.2° E. This suggests that the SLA at that location is a reasonable proxy for the KC transport variability through the East Taiwan Channel and can be used as a zero order predictor for the KC–ECS interaction events (Vélez-Belchí et al., 2013).

5. APPLICATIONS

Knowing surface currents is important for many applications. Since 1992, a constellation of satellite altimeters monitors the shape of the ocean surface with an accuracy and resolution sufficient to resolve large oceanic eddies (Pascual et al., 2006) and major ocean currents. Sea-level data are used in circulation and climate studies and are assimilated in many ocean models, including operational current forecast systems designed during the Global Ocean Data Assimilation Experiment (GODAE). For the latter models, other direct current datasets are also used for assimilation, such as high-frequency radar (HFR) and Autonomous Doppler Current Profiler (ADCP) observations (Davidson et al., 2009). Velocity data from Lagrangian drifters, however, are not suitable for operational oceanography because the drogue detection algorithm and sensors do not currently work in real time. Drifter velocity data, on the other hand, are one of the few independent datasets available to validate outputs from ocean forecasts (Hurlburt et al., 2009). For example, they are used to validate the Mercator Océan NEMO global model (Lellouche et al., 2013). In delayed mode, drifter velocities are also important for an accurate sea state estimate (Wunsch et al., 2009) facilitating the use of satellite-measured anomalies and, in the end, increasing forecast quality.

Operational surface current products, available from a number of teams, are actively used for tracking oil spills (c.f., Hackett et al., 2009), search and rescue, and ship routing (Davidson et al., 2009), maritime safety and iceberg drift, larval dispersal and harmful algal blooms (De Mey et al., 2009) and by the Navy for maritime operations (Jacobs et al., 2009).

One emerging application is to study the dynamics of marine debris. The trajectory of an object floating on the surface of the ocean is set by currents, waves, and wind, and depends on the geometry and mass distribution of the object. Light flotsam such as balloons are mainly blown by wind, while heavy objects, such as the GDP drifters, derelict fishing gear, and ship wrecks are mainly carried by currents. This latter group also includes

microplastic, tiny pieces, produced by breaking old plastic, which can survive in water for many decades. This class of debris represents the most common type of marine debris, which poses the greatest risks for navigational safety and the health of the marine ecosystem. Because vertical excursions of flotsam are suppressed by their buoyancy, floating debris accumulates in open-ocean and coastal regions of downwelling.

The GDP dataset provides rich information about the pathways of marine debris. The main pathways are well represented by the mean streamlines, shown in Figure 12.2a. To eliminate the bias existing in drifter statistics due to highly heterogeneous density of the drifter ensemble, Maximenko et al. (2012) developed a statistical model, based on probability of observed drifter excursion between different boxes. Lumpkin et al. (2011) developed a technique to assess the probability that a drifter will run aground on different parts of the coastline. This model, accounting for probabilistic displacements of particles and their chance to end on the coast, was used for a numerical experiment with an initially homogeneous density of marine debris (Lumpkin et al., 2011). Figure 12.7 shows that after 10 years of wandering around the ocean, most of the debris (nearly 70% of the initial mass) is still floating, collected in five subtropical "garbage patches." While the North Pacific (Moore et al., 2001) and North Atlantic (Law et al., 2010) garbage patches are well known, three others have been confirmed only recently (Eriksen et al., 2013) and are being currently documented by researchers. Vertical bars on Figure 12.7 show the global pattern of "clean" and "dirty" shores, correlating well with the direction of dominant winds.

Another experiment with the same model can simulate the motion of debris generated on the northeastern coast of Japan. This helps to statistically predict the fate of debris originating from the tsunami of March 11, 2011. Figure 12.8 illustrates that debris will likely disperse over large area and the center of mass of the debris field will first drift toward east and later will recirculate into the garbage patch. Two and a half years after tsunami, scarce reports from sea generally confirm predictions of the model. Their analysis emphasizes importance of wind force, acting on high-windage objects, which are the most visible members of the debris ensemble at rough sea.

6. FUTURE DIRECTIONS

Important advances in our ability to observe surface currents have been made in recent decades. With the help of the GOOS, including the network of the GDP drifters and satellite altimeters, surface currents are monitored on space scales larger than 100 km and timescales longer than one week. These observations are complemented by satellite-borne measurements of the geoid and of surface winds, particularly via scatterometers, to separately resolve the geostrophic and ageostrophic components of surface currents. These observations provide invaluable information for basic and applied research on the ocean and climate dynamics. Yet, most operational activity requires resolution of a few kilometers delivered to the user within hours. The importance of smaller scales is not only in better description of details of ocean currents. The submesoscale contains most vertical motions, sustaining life in the upper

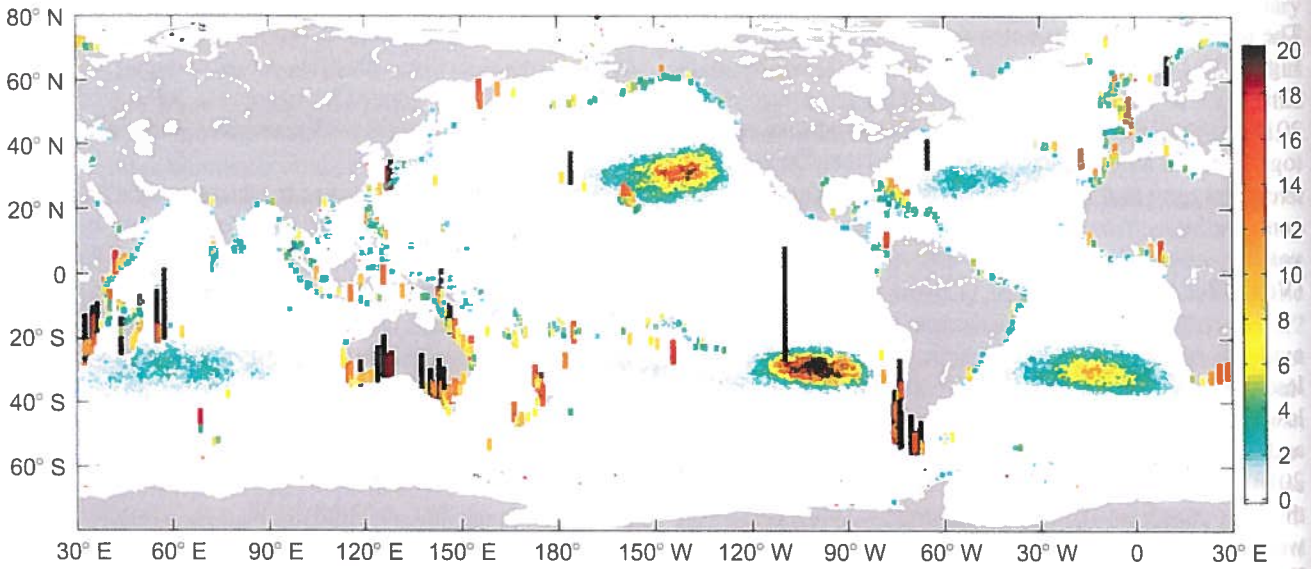

FIGURE 12.7 Distribution of the concentration of floating marine debris in arbitrary units, after 10 years of integration from an initially homogeneous distribution of concentration unity. Vertical bars indicate the concentration of material that has washed ashore, with color corresponding to 10 times the value in the color bar. *Reproduced from Lumpkin et al. (2011).*

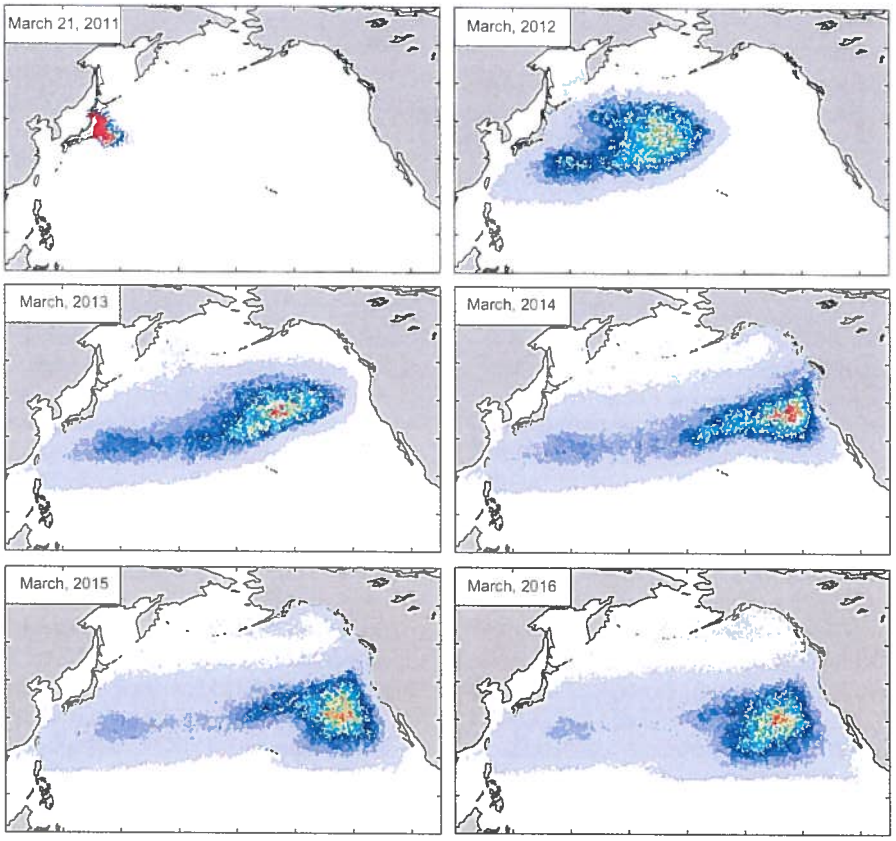

FIGURE 12.8 The probable pathways of the debris from the March 11, 2011 tsunami in Japan as estimated from historical trajectories of drifting buoys. *Reproduced from Maximenko et al. (2011).*

ocean (c.f., Klein et al., 2008; Lapeyre, 2009). Upwelling in local fronts commonly induces chlorophyll blooms, in which complex ecosystems quickly build up. Downwellings, on the contrary, are generated by surface convergences and collect marine debris and other floating pollutants. Experiments with ultra-high-resolution models also indicate that the vorticity of ocean currents, whose balance plays a principal role in the dynamics of ocean circulation, varies on scales of kilometers or less. Fine resolution will also allow expanding observations closer to the shore, the area of the greatest interest of most users. NASA's Surface Water Ocean Topography (SWOT) mission will approach these parameters using a wide-swath interferometry between a pair of radar altimeters, installed on a single satellite. The launch of SWOT is planed after 2020. Drifters, measuring full velocity, will be essential for future studies of submesoscale processes. At the same time, while increased resolution and accuracy along the trajectory are feasible thanks to new satellite systems (e.g., Iridium and GPS), implementing and maintaining a drifter array with submesoscale coverage is still a task for the future.

Conversion of the sea-level signal into velocity is not straightforward on small scales, where geostrophic Equation (12.1) is not a good approximation. New techniques (such as surface quasi-geostrophy (SQG) (Klein et al., 2008)) will need to be developed and implemented that will require better understanding of the momentum balance in the upper ocean. Velocities, measured with the array of GDP drifters (after some corrections for the wind-forced slip), are interpreted as ocean currents at a nominal depth of 15 m. Neither the motion of the drogue in rough seas where the wave height is a significant fraction of the drogue's depth nor much details of the upper-ocean velocity shear are well documented. No model or theory existing today approaches the full complexity of surface currents, and the very definition of the "sea surface" in the presence of breaking waves is far from trivial. For example, Kudryavtsev et al. (2008) point out inconsistencies of modern models of the mixed layer and suggest the wind force is not just applied at the sea surface, but momentum may be "injected" into deeper layers by breaking wind waves. Validation of this idea and progress in understanding the details of the momentum balance will require implementation in large numbers of existing velocity profilers and development of new, more efficient technologies.

New technologies are also required to monitor near-surface currents covered by ice. Implementation of engineering ideas (Freeman et al., 2010), allowing remote sensing of the ocean surface velocity vector with satellite, would further revolutionize the science of the upper ocean.

Gaps in observations of ocean currents can be filled using models of different complexity, synthesizing other datasets, from diagnostic models combining in a simple way wind- and pressure-driven velocities (e.g., Uchida and Imawaki (2003); OSCAR (Bonjean and Lagerloef, 2002); SCUD (Maximenko and Hafner, 2010)) to data assimilating systems (e.g., ECCO (Wunsch et al., 2009); HYCOM (Chassignet et al., 2009)). Enhancement of the observational dataset of surface velocity will help to validate and improve these models.

ACKNOWLEDGMENTS

N. M. was partly supported by NASA Ocean Surface Topography Science Team through Grants NNX08AR49G and NNX13AK35G, and also by JAMSTEC, by NASA through Grant NNX07AG53G, and by NOAA through Grant NA11NMF4320128 through their sponsorship of the International Pacific Research Center. R. L. was supported by NOAA's Office of Climate Observations and the Atlantic Oceanographic and Meteorological Laboratory. L. C. was supported by NOAA's Office of Climate Observations and by the Office of Naval Research. IPRC/SOEST Publication 962/8896.

REFERENCES

Alford, M.H., Whitmont, M., 2007. Seasonal and spatial variability of near-inertial kinetic energy from historical moored velocity records. J. Phys. Oceanogr. 37 (8), 2022–2037.

Archiving, Validation, and Interpretation of Satellite Oceanographic Data (Aviso), 1996. Aviso Handbook for Merged TOPEX/Poseidon Products, third ed. Aviso, Toulouse, France.

Austin, J.A., Barth, J.A., 2002. Drifter behavior on the Oregon-Washington shelf during downwelling-favorable winds. J. Phys. Oceanogr. 32 (11), 3132–3144.

Baldwin, M.P., Rhines, P.B., McIntyre, M.E., 2007. The jet-stream conundrum. Science 315, 467–468.

Bhatt, U.S., 1989. Circulation regimes of rainfall anomalies in the African South Asian monsoon belt. J. Clim. 2 (10), 1133–1144.

Boebel, O., Rossby, T., Lutjeharms, J., Zenk, W., Barron, C., 2003. Path and variability of the Agulhas return current. Deep Sea Res. Part II 50, 35–56.

Bonjean, F., Lagerloef, G., 2002. Diagnostic model and analysis of the surface currents in the tropical Pacific Ocean. J. Phys. Oceanogr. 32, 2938–2954.

Brambilla, E., Talley, L., 2006. Surface drifter exchange between North Atlantic subtropical and subpolar gyres. J. Geophys. Res. 111, C07026. http://dx.doi.org/10.1029/2005JC003146.

Brink, K.H., Beardsley, R.C., Niiler, P.P., Abbott, M., Huyer, A., Ramp, S., Stanton, T., Stuart, D., 1991. Statistical properties of near-surface flow in the California coastal transition zone. J. Geophys. Res. 96, 14693–14706.

Buckingham, C.E., Cornillon, P.C., 2013. The contribution of eddies to striations in absolute dynamic topography. J. Geophys. Res. Oceans 118, 448–461. http://dx.doi.org/10.1029/2012JC008231.

Centurioni, L.R., Niiler, P.P., Lee, D.K., 2004. Observations of inflow of Philippine Sea surface water into the South China Sea through the Luzon Strait. J. Phys. Oceanogr. 34 (1), 113–121.

Centurioni, L.R., Niiler, P.P., Kim, Y.Y., Sheremet, V.A., Lee, D.K., 2007. Near surface dispersion of particles in the South China Sea. In: Griffa, A.D.K.A., Mariano, A.J., Özgökmen, T., Rossby, T. (Eds.), Lagrangian Analysis and Prediction of Coastal and Ocean Dynamics. Cambridge University Press, pp. 73–75.

Centurioni, L.R., Ohlmann, J.C., Niiler, P.P., 2008. Permanent meanders in the California current system. J. Phys. Oceanogr. 38 (8), 1690–1710.

Centurioni, L.R., Niiler, P.P., Lee, D.K., 2009. Near-surface circulation in the South China Sea during the winter monsoon. Geophys. Res. Lett. 36, L06605. http://dx.doi.org/10.1029/02008GL037076.

Chaigneau, A., Pizarro, O., Rojas, W., 2008. Global climatology of near-inertial current characteristics from Lagrangian observations. Geophys. Res. Lett. 35, L13603. http://dx.doi.org/10.1029/2008GL034060.

Chassignet, E.P., Hurlburt, H.E., Metzger, E.J., Smedstad, O.M., Cummings, J., Halliwell, G.R., Bleck, R., Baraille, R., Wallcraft, A.J., Lozano, C., Tolman, H.L., Srinivasan, A., Hankin, S., Cornillon, P., Weisberg, R., Barth, A., He, R., Werner, F., Wilkin, J., 2009. U.S. GODAE: global ocean prediction with the HYbrid Coordinate Ocean Model (HYCOM). Oceanography 22 (2), 64–75.

Chelton, D.B., Schlax, M.G., Samelson, R.M., 2011. Global observations of nonlinear mesoscale eddies. Prog. Oceanog. 91, 167–216. http://dx.doi.org/10.1016/j.pocean.2011.01.002.

Chen, C.T.A., 2005. Tracing tropical and intermediate waters from the South China Sea to the Okinawa Trough and beyond. J. Geophys. Res. Oceans 110 (C5), C05012. http://dx.doi.org/10.1029/2004JC002494.

Chen, C.-T.A., Huang, M.-H., 1996. A mid-depth front separating the South China Sea water and the Philippine Sea water. J. Oceanogr. 52 (1), 17–25.

Chereskin, T.K., 1995. Evidence for an Ekman balance in the California Current. J. Geophys. Res. 100, 12727–12748.

Chereskin, T.K., Morris, M.Y., Niiler, P.P., Kosro, P.M., Smith, R.L., Ramp, S.R., Collins, C.A., Musgrave, D.L., 2000. Spatial and temporal characteristics of the mesoscale circulation of the California Current from eddy-resolving moored and shipboard measurements. J. Geophys. Res. Oceans 105 (C1), 1245–1269.

Cornuelle, B.D., Chereskin, T.K., Niiler, P.P., Morris, M.Y., Musgrave, D. L., 2000. Observations and modeling of a California undercurrent eddy. J. Geophys. Res. 105 (C1), 1227–1243.

Davidson, F.J.M., Allen, A., Brassington, G.B., Breivik, O., Daniel, P., Kamachi, M., Sato, S., King, B., Lefevre, F., Sutton, M., Kaneko, H., 2009. Applications of GODAE ocean current forecasts to search and rescue and ship routing. Oceanography 22 (3), 176–181. http://dx.doi.org/10.5670/oceanog.2009.76.

Davis, R.E., 1985a. Drifter observations of coastal surface currents during CODE—the method and descriptive view. J. Geophys. Res. 90 (C3), 4741–4755.

Davis, R.E., 1985b. Drifter observations of coastal surface currents during CODE: the statistical and dynamical views. J. Geophys. Res. 90 (C3), 4756–4772.

Davis, R., 1991. Observing the general circulation with floats. Deep Sea Res. 38, S531–S571.

De Mey, P., Craig, P., Davidson, F., Edwards, C.A., Ishikawa, Y., Kindle, J.C., Proctor, R., Thompson, K.R., Zhu, J., the GODAE Coastal and Shelf Seas Working Group (CSSWG) Community, 2009. Applications in coastal modeling and forecasting. Oceanography 22 (3), 98–205. http://dx.doi.org/10.5670/oceanog.2009.79.

Ducet, N., Le Traon, P.Y., Reverdin, G., 2000. Global high-resolution mapping of ocean circulation from TOPEX/Poseidon and ERS-1 and -2. J. Geophys. Res. 105 (C8), 19477–19489.

Ekman, V.W., 1905. On the influence of the earth's rotation on ocean currents. Arch. Math. Astron. Phys. 2 (11), 1–52.

Elipot, S., Lumpkin, R., 2008. Spectral description of oceanic near-surface variability. Geophys. Res. Lett. 35, L05606. http://dx.doi.org/10.1029/2007GL032874.

Elipot, S., Lumpkin, R., Prieto, G., 2010. Modification of inertial oscillations by the mesoscale eddy field. J. Geophys. Res. 115, C09010. http://dx.doi.org/10.1029/2009JC005679.

Eriksen, M., Maximenko, N.A., Thiel, M., Cummins, A., Lattin, G., Wilson, S., Hafner, J., Zellers, A., Rifman, S., 2013. Plastic pollution in the South Pacific subtropical gyre. Mar. Pollut. Bull. 68, 71–76. http://dx.doi.org/10.1016/j.marpolbul.2012.12.021.

Franklin, B., 1785. Sundry marine observations. Trans. Am. Philos. Soc. Ser. 1 2, 294–329.

Fratantoni, D.M., 2001. North Atlantic surface circulation during the 1990's observed with satellite-tracked drifters. J. Geophys. Res. 106, 22067–22093. http://dx.doi.org/10.1029/2000JC000730.

Freeland, H.J., Rhines, P., Rossby, H.T., 1975. Statistical observations of trajectories of neutrally buoyant floats in the North Atlantic. J. Mar. Res. 33, 383–404.

Freeman, A., Zlotnicki, V., Liu, T., Fu, L.-L., Holt, B., Kwok, R., Yueh, S., Fukumori, I., Vazquez, J., Siegel, D., Lagerloef, G., 2010. Ocean measurements from space in 2025. Oceanography 23 (4), 144–161.http://dx.doi.org/10.5670/oceanog.2010.12.

Galperin, B., Nakano, H., Huang, H.-P., Sukoriansky, S., 2004. The ubiquitous zonal jets in the atmospheres of giant planets and Earth's oceans. Geophys. Res. Lett. 31, L13303. http://dx.doi.org/10.1029/2004GL019691.

Garrett, J.F., 1980. The availability of the FGGE drifting buoy system data set. Deep Sea Res. 27, 1083–1086.

Gawarkiewicz, G., Jan, S., Lermusiaux, P.F.J., McClean, J.L., Centurioni, L., Taylor, K., Cornuelle, B., Duda, T.F., Wang, J., Yang, Y.J., Sanford, T., Lien, R.-C., Lee, C., Lee, M.-A., Leslie, W., Haley Jr., P.J., Niiler, P.P., Gopalakrishnan, G., Velez-Belchi, P., Lee, D.-K., Kim, Y.Y., 2011. Circulation and intrusions Northeast of Taiwan: chasing and predicting uncertainty in the cold dome. Oceanography 24 (4), 110–121. http://dx.doi.org/10.5670/oceanog.2011.99.

Gill, A., 1982. Atmosphere-Ocean Dynamics. Elsevier, 662 pp.

Grodsky, S.A., Lumpkin, R., Carton, J.A., 2011. Spurious trends in global surface drifter currents. Geophys. Res. Lett. 38, L10606. http://dx.doi.org/10.1029/2011GL047393.

Hackett, B., Comerma, E., Daniel, P., Ichikawa, H., 2009. Marine oil pollution prediction. Oceanography 22 (3), 168–175. http://dx.doi.org/10.5670/oceanog.2009.75.

Haines, K., Johannessen, J.A., Knudsen, P., Lea, D., Rio, M.-H., Bertino, L., Davidson, F., Hernandez, F., 2011. An ocean modelling and assimilation guide to using GOCE geoid products. Ocean Sci. 7, 151–164. http://dx.doi.org/10.5194/os-7-151-2011.

Hansen, D.V., Poulain, P.-M., 1996. Quality control and interpolations of WOCE-TOGA drifter data. J. Atmos. Oceanic Technol. 13, 900–909.

Hofmann, E.E., Worley, S.J., 1986. An investigation of the circulation of the Gulf of Mexico. J. Geophys. Res. 91 (C12), 14221–14236.

Hu, J., Kawamura, H., Hong, H., Qi, Y., 2000. A review on the Currents in the South China Sea: seasonal circulation South China sea warm current and Kuroshio intrusion. J. Oceanogr. 56 (6), 607–624.

Huang, H.-P., Kaplan, A., Curchitser, E.N., Maximenko, N.A., 2007. The degree of anisotropy for mid-ocean currents from satellite observations and an eddy-resolving model simulation. J. Geophys. Res. Oceans 112, C09005. http://dx.doi.org/10.1029/2007JC004105.

Hughes, C.W., 2005. Nonlinear vorticity balance of the Antarctic Circumpolar Current. J. Geophys. Res. 110, C11008. http://dx.doi.org/10.1029/2004JC002753.

Hurlburt, H.E., Brassington, G.B., Drillet, Y., Kamachi, M., Benkiran, M., Bourdallé-Badie, R., Chassignet, E.P., Jacobs, G.A., Le Galloudec, O., Lellouche, J.-M., Metzger, E.J., Oke, P.R., Pugh, T.F., Schiller, A., Smedstad, O.M., Tranchant, B., Tsujino, H., Usui, N., Wallcraft, A.J., 2009. High-resolution global and basin-scale ocean analyses and forecasts. Oceanography 22 (3), 110–127. http://dx.doi.org/10.5670/oceanog.2009.70.

Huyer, A., 1983. Coastal upwelling in the California current system. Prog. Oceanogr. 12 (3), 259–284.

Imawaki, S., Uchida, H., Ichikawa, H., Fukasawa, M., Umatani, S., ASUKA Group, 2001. Satellite altimeter monitoring the Kuroshio transport South of Japan. Geophys. Res. Lett. 28 (1), 17–20.

Imawaki, S., Uchida, H., Ichikawa, K., Ambe, D., 2003. Estimating the high-resolution mean sea-surface velocity field by combined use of altimeter and drifter data for geoid model improvement. Space Sci. Rev. 108, 195–204.

Jacobs, G.A., Woodham, R., Jourdan, D., Braithwaite, J., 2009. GODAE applications useful to navies throughout the world. Oceanography 22 (3), 182–189. http://dx.doi.org/10.5670/oceanog.2009.77.

Johannessen, J.A., Balmino, G., Le Provost, C., Rummel, R., Sabadini, R., Sunkel, H., Tscherning, C.C., Visser, P., Woodworth, P., Hughes, C. W., LeGrand, P., Sneeuw, N., Perosanz, F., Aguirre-Martinez, M., Rebhan, H., Drinkwater, M., 2003. The European gravity field and steady-state ocean circulation explorer satellite mission: impact in geophysics. Surv. Geophys. 24, 339–386.

Johns, W.E., Lee, T.N., Zhang, D.X., Zantopp, R., Liu, C.T., Yang, Y., 2001. The Kuroshio east of Taiwan: moored transport observations from the WOCE PCM-1 array. J. Phys. Oceanogr. 31 (4), 1031–1053.

Kida, S., Price, J.F., Jiayan, Y., 2007. The upper-oceanic response to overflows: a mechanism for the Azores Current. J. Phys. Oceanogr. 38, 880–895.

Klein, B., Siedler, G., 1989. On the origin of the Azores Current. J. Geophys. Res. 94, 6159–6168.

Klein, P., Hua, B.L., Lapeyre, G., Capet, X., Le Gentil, S., Sasaki, H., 2008. Upper ocean turbulence from high-resolution 3D simulations. J. Phys. Oceanogr. 38, 1748–1763.

Knudsen, P., Bingham, R., Andersen, O.B., Rio, M.-H., 2011. Enhanced mean dynamic topography and ocean circulation estimation using GOCE preliminary models. In: Presentataion at the 4th International GOCE User Workshop, 31 March–01 April 2011, Munich, Germany, Available at: https://earth.esa.int/download/goce/4th_Int_GOCE_User_Wkshp_2011/Enhanced_Mean_Dynamic_Topography_P.Knudsen.pdf.

Krauss, W., Böning, C., 1987. Lagrangian properties of eddy fields in the northern North Atlantic as deduced from satellite-tracked buoys. J. Mar. Res. 45, 259–291.

Kudryavtsev, V., Shrira, V., Dulov, V., Malinovsky, V., 2008. On the vertical structure of wind-driven sea currents. J. Phys. Oceanogr. 38, 2121–2144.

Kunze, E., 1985. Near-inertial wave propagation in geostrophic shear. J. Phys. Oceanogr. 15 (5), 544–565.

LaCasce, J.H., Ohlmann, C., 2003. Relative dispersion at the surface of the Gulf of Mexico. J. Mar. Res. 61 (3), 285–312.

Lapeyre, G., 2009. What vertical mode does the altimeter reflect? On the decomposition in baroclinic modes and on a surface-trapped mode. J. Phys. Oceanogr. 39, 2857–2874.

Law, K.L., Morét-Ferguson, S., Maximenko, N.A., Proskurowski, G., Peacock, E.E., Hafner, J., Reddy, C.M., 2010. Plastic accumulation in the North Atlantic Subtropical Gyre. Science 329, 1185–1188.

Le Traon, P.-Y., Schaeffer, P., Guinehut, S., Rio, M.-H., Hernandez, F., Larnicol, G., Lemoine, J.M., 2001. Mean ocean dynamic topography from GOCE and altimetry. In: Proceedings of the 1st International GOCE Workshop, April 23–24. ESTEC, Noordwijk, The Netherlands. Available at: http://earth.esa.int/goce04/first_igw/papers/Letraon_etal.pdf.

Lee, D.-K., Niiler, P.P., 1998. The inertial chimney: the near-inertial energy drainage from the ocean surface to the deep layer. J. Geophys. Res. 103 (C4), 7579–7591.

Lee, D.K., Niiler, P., Warnvarnas, A., Piacsek, S., 1994. Wind-driven secondary circulation in ocean mesoscale. J. Mar. Res. 52 (3), 371–396.

Lellouche, J.-M., Le Galloudec, O., Drévillon, M., Régnier, C., Greiner, E., Garric, G., Ferry, N., Desportes, C., Testut, C.-E., Bricaud, C., Bourdallé-Badie, R., Tranchant, B., Benkiran, M., Drillet, Y., Daudin, A., De Nicola, C., 2013. Evaluation of global monitoring and forecasting systems at Mercator Océan. Ocean Sci. 9, 57–81. http://dx.doi.org/10.5194/os-9-57-2013.

Li, L., Qu, T., 2006. Thermohaline circulation in the deep South China Sea basin inferred from oxygen distributions. J. Geophys. Res. 111, C05017. http://dx.doi.org/10.1029/2005JC003164.

Liu, Q.Y., Jiang, X., Xie, S.P., Liu, W.T., 2004. A gap in the Indo-Pacific warm pool over the South China Sea in boreal winter: seasonal development and interannual variability. J. Geophys. Res. Oceans 109, C07012.

Lumpkin, R., Garzoli, S.L., 2005. Near-surface circulation in the tropical Atlantic Ocean. Deep Sea Res. Part I 52, 495–518. http://dx.doi.org/10.1016/j.dsr.2004.09.001.

Lumpkin, R., Garzoli, S., 2010. Interannual to decadal changes in the Southwestern Atlantic's surface circulation. J. Geophys. Res. Oceans 116, C01014. http://dx.doi.org/10.1029/2010JC006285.

Lumpkin, R., Goni, G., Dohan, K., 2009. State of the ocean in 2008: surface currents. In: Peterson, T., Baringer, M. (Eds.), State of the Climate in 2008, vol. 90. Bulletin of the American Meteorological Society, pp. S12–S15.

Lumpkin, R., Maximenko, N., Pazos, M., 2011. Evaluating where and why drifters die. J. Atmos. Oceanic Technol. 29, 300–308. http://dx.doi.org/10.1175/JTECH-D-11-00100.1.

Lumpkin, R., Grodsky, S., Rio, M.-H., Centurioni, L., Carton, J., Lee, D., 2013. Removing spurious low-frequency variability in surface drifter velocities. J. Atmos. Oceanic Technol. 30 (2), 353–360. http://dx.doi.org/10.1175/JTECH-D-12-00139.1.

Marchesiello, P., McWilliams, J.C., Shchepetkin, A., 2003. Equilibrium structure and dynamics of the California Current System. J. Phys. Oceanogr. 33 (4), 753–783.

Maximenko, N., 2004. Correspondence between Lagrangian and Eulerian velocity statistics at the ASUKA line. J. Oceanogr. 60 (4), 681–687.

Maximenko, N., Hafner, J., 2010. SCUD: Surface CUrrents from Diagnostic model. IPRC Technical Note, No. 5, February 16, 2010, 17 p.

Maximenko, N.A., Niiler, P.P., 2005. Hybrid decade-mean global sea level with mesoscale resolution. In: Saxena, N.K. (Ed.), Recent Advances in Marine Science and Technology 2004. PACON International, Honolulu, Hawaii, pp. 55–59.

Maximenko, N.A., Niiler, P.P., 2006. Mean surface circulation of the global ocean inferred from satellite altimeter and drifter data. In: 15 Years of Progress in Radar Altimetry, ESA Publication SP-614, July 2006.

Maximenko, N.A., Bang, B., Sasaki, H., 2005. Observational evidence of alternating zonal jets in the world ocean. Geophys. Res. Lett. 32, L12607. http://dx.doi.org/10.1029/2005GL022728.

Maximenko, N.A., Melnichenko, O.V., Niiler, P.P., Sasaki, H., 2008. Stationary mesoscale jet-like features in the ocean. Geophys. Res. Lett. 35, L08603. http://dx.doi.org/10.1029/2008GL033267.

Maximenko, N., Niiler, P., Centurioni, L., Rio, M.-H., Melnichenko, O., Chambers, D., Zlotnicki, V., Galperin, B., 2009. Mean dynamic topography of the ocean derived from satellite and drifting buoy data using three different techniques. J. Atmos. Oceanic Technol. 26 (9), 1910–1919.

Maximenko, N., Hafner, J., Lumpkin, R., 2011. Modeling distribution of marine debris before and after tsunami of March 11, 2011. In: Presentation at the Ocean Surface Topography Science Team Meeting, San Diego, California, October 19–21. http://www.aviso.oceanobs.com/fileadmin/documents/OSTST/2011/oral/.

Maximenko, N., Hafner, J., Niiler, P., 2012. Pathways of marine debris from trajectories of Lagrangian drifters. Mar. Pollut. Bull. 65, 51–62. http://dx.doi.org/10.1016/j.marpolbul.2011.04.016.

McNally, G.J., Patzert, W.C., Kirwan, J.A.D., Vastano, A.C., 1983. The near-surface circulation of the North Pacific using satellite tracked drifting buoys. J. Geophys. Res. 88, 7634–7640.

Melnichenko, O.V., Maximenko, N.A., Schneider, N., Sasaki, H., 2010. Quasi-stationary striations in basin-scale oceanic circulation: vorticity balance from observations and eddy-resolving model. Ocean Dyn. 60 (3), 653–666.

Moore, C., Moore, S.L., Leecaster, M.K., Weisberg, S.B., 2001. A comparison of plastic and plankton in the north pacific central gyre. Mar. Pollut. Bull. 42, 1297–1300. http://dx.doi.org/10.1016/S0025-326X(01)00114-X, 2001-12-01.

Munk, W.H., Wunsch, C., 1998. Abyssal recipes II: energetics of tidal and wind mixing. Deep Sea Res. Part I 45, 1977–2010.

Nakano, H., Hasumi, H., 2005. A series of zonal jets embedded in the broad zonal flows in the Pacific obtained in eddy-permitting ocean general circulation models. J. Phys. Oceanogr. 35, 474–488.

Needler, G., Smith, N., Villwock, A., 1999. The Action Plan for GOOS/GCOS and Sustained Observations for CLIVAR. Available at: http://www.oceanobs09.net/work/oo99/docs/Needler.pdf.

Niiler, P., 2001. The world ocean surface circulation. In: Siedler, G., Church, J., Gould, J. (Eds.), Ocean Circulation and Climate. International Geophysics Series, vol. 77. Academic Press, pp. 193–204.

Niiler, P.P., 2003. A brief history of drifter technology. In: Autonomous and Lagrangian Platforms and Sensors Workshop. Scripps Institution of Oceanography, La Jolla, CA.

Niiler, P.P., Paduan, J.D., 1995. Wind-driven motions in the northeast Pacific as measured by Lagrangian drifters. J. Phys. Oceanogr. 25, 2819–2830.

Niiler, P.P., Davis, R., White, H., 1987. Water-following characteristics of a mixed-layer drifter. Deep Sea Res. 34, 1867–1882.

Niiler, P.P., Sybrandy, A., Bi, K., Poulain, P., Bitterman, D., 1995. Measurements of the water-following capability of holey-sock and TRISTAR drifters. Deep Sea Res. 42, 1951–1964.

Niiler, P.P., Maximenko, N.A., Panteleev, G.G., Yamagata, T., Olson, D. B., 2003a. Near-surface dynamical structure of the Kuroshio

Extension. J. Geophys. Res. 108, 3193. http://dx.doi.org/10.1029/2002JC001461.

Niiler, P.P., Maximenko, N.A., McWilliams, J.C., 2003b. Dynamically balanced absolute sea level of the global ocean derived from near-surface velocity observations. Geophys. Res. Lett. 30, 2164. http://dx.doi.org/10.1029/2003GL018628.

Nitani, H., 1972. Beginning of the Kuroshio. In: Stommel, H., Yoshida, K. (Eds.). Kuroshio: Its Physical Aspects. University of Tokyo Press, pp. 129–163.

Paduan, J.D., Niiler, P.P., 1993. Structure of velocity and temperature in the Northeast Pacific as measured with Lagrangian drifters in Fall 1987. J. Phys. Oceanogr. 23, 585–600.

Pascual, A., Faugère, Y., Larnicol, G., Le Traon, P.-Y., 2006. Improved description of the ocean mesoscale variability by combining four satellite altimeters. Geophys. Res. Lett. 33, L02611. http://dx.doi.org/10.1029/2005GL024633.

Pazan, S.E., Niiler, P.P., 2001. Recovery of near-surface velocity from undrogued drifters. J. Atmos. Oceanic Technol. 18, 476–489.

Pazan, S.E., Niiler, P.P., 2004. New global drifter data set available. Eos 85, 17.

Pedlosky, J., 1996. Ocean Circulation Theory. Springer-Verlag, Berlin, pp. 405–409.

Polzin, K., 2008. Mesoscale eddy–internal wave coupling. Part I: symmetry, wave capture and results from the mid-ocean dynamics experiment. J. Phys. Oceanogr. 38 (11), 2556–2574.

Poulain, P.M., Niiler, P.P., 1989. Statistical-analysis of the surface circulation in the California current system using satellite-tracked drifters. J. Phys. Oceanogr. 19 (10), 1588–1603.

Qiu, B., Chen, S., 2005. Variability of the Kuroshio Extension Jet, recirculation gyre, and mesoscale eddies on decadal time scales. J. Phys. Oceanogr. 35, 2090–2103.

Qu, T.D., 2000. Upper-layer circulation in the South China Sea. J. Phys. Oceanogr. 30 (6), 1450–1460.

Ralph, E.A., Niiler, P.P., 1999. Wind-driven currents in the tropical Pacific. J. Phys. Oceanogr. 29 (9), 2121–2129.

Reverdin, G., Frankignoul, C., Kestenare, E., McPhaden, M.J., 1994. Seasonal variability in the surface currents of the equatorial Pacific. J. Geophys. Res. 99, 20323–20344.

Rhines, P.B., 1975. Waves and turbulence on a beta-plane. J. Fluid Mech. 69, 417–443.

Richards, K.J., Maximenko, N.A., Bryan, F.O., Sasaki, H., 2006. Zonal jets in the Pacific Ocean. Geophys. Res. Lett. 33, L03605. http://dx.doi.org/10.1029/2005GL024645.

Richardson, P., 1980. Gulf Stream ring trajectories. J. Phys. Oceanogr. 10, 90–104.

Richardson, P.L., McKee, T.K., 1984. Average seasonal variation of the Atlantic equatorial currents from historical ship drift. J. Phys. Oceanogr. 14, 1226–1238.

Richardson, P., Reverdin, G., 1987. Seasonal cycle of velocity in the Atlantic North Equatorial Countercurrent as measured by surface drifters, current meters, and ship drifts. J. Geophys. Res. 92, 3691–3708.

Richardson, P., Walsh, D., 1986. Mapping climatological seasonal variations of surface currents in the Tropical Atlantic using ship drifts. J. Geophys. Res. 91, 10537–10550.

Rio, M.H., 2012. Use of Altimeter and Wind Data to Detect the Anomalous Loss of SVP-Type Drifter's Drogue. J. Atmos. Oceanic Technol. 29, 1663–1674. http://dx.doi.org/10.1175/JTECH-D-12-00008.1.

Rio, M.H., Hernandez, F., 2003. High-frequency response of wind-driven currents measured by drifting buoys and altimetry over the world ocean. J. Geophys. Res. 108 (C8), 3283. http://dx.doi.org/10.1029/2002JC001655.

Rio, M.H., Hernandez, F., 2004. A mean dynamic topography computed over the world ocean from altimetry, in situ measurements, and a geoid model. J. Geophys. Res. 109, C12032. http://dx.doi.org/10.1029/2003JC002226.

Rio, M.H., Guinehut, S., Larnicol, G., 2011a. New CNES-CLS09 global mean dynamic topography computed from the combination of GRACE data, altimetry, and in situ measurements. J. Geophys. Res. 116, C07018. http://dx.doi.org/10.1029/2010JC006505.

Rio, M.-H., Mulet, S., Guinehut, S., Lambin, J., Bronner, E., 2011b. High-resolution mean dynamic topography in the Kerguelen area from altimetry, GOCE data, and oceanographic in situ measurements. In: Presentation at the OSTST meeting, October 20, 2011, San Diego, USA. Available at: http://www.aviso.oceanobs.com/fileadmin/documents/OSTST/2011/oral/02_Thursday/Splinter%202%20GEO/03%20Helene%20%20Rio%20rev%20MDT_KEOPS_rio.pdf.

Romanou, A., Chassignet, E.P., Sturges, W., 2004. Gulf of Mexico circulation within a high-resolution numerical simulation of the North Atlantic Ocean. J. Geophys. Res. Oceans 109, C01003. http://dx.doi.org/10.1029/2003JC001770.

Roy, C., Reason, C., 2001. ENSO related modulation of coastal upwelling in the eastern Atlantic. Prog. Oceanogr. 49 (1–4), 245–255.

Rudnick, D.L., Jan, S., Centurioni, L., Lee, C.M., Lien, R.-C., Wang, J., Lee, D.-K., Tseng, R.-S., Kim, Y.Y., Chern, C.-S., 2011. Seasonal and mesoscale variability of the Kuroshio near its origin. Oceanography 24 (4), 52–63.

Sasaki, H., Nonaka, M., 2006. Far-reaching Hawaiian Lee Countercurrent driven by wind-stress curl induced by warm SST band along the current. Geophys. Res. Lett. 33, L13602. http://dx.doi.org/10.1029/2006GL026540.

Schlax, M.G., Chelton, D.B., 2008. The influence of mesoscale eddies on the detection of quasi-zonal jets in the ocean. Geophys. Res. Lett. 35, L24602. http://dx.doi.org/10.1029/2008GL035998.

Scott, R.B., Arbic, B.K., Holland, C.L., Sen, A., Qiu, B., 2008. Zonal versus meridional velocity variance in satellite observations and realistic and idealized ocean circulation models. Ocean Model. 23, 102–112.

Strub, P.T., Kosro, P.M., Huyer, A., 1991. The nature of the cold filaments in the California Current System. J. Geophys. Res. Oceans 96 (C8), 14743–14768.

Sverdrup, H.U., 1947. Wind-driven currents in a baroclinic ocean; with application to the equatorial currents of the eastern Pacific. Proc. Natl. Acad. Sci. U.S.A. 33, 318–326.

Sverdrup, H.U., Johnson, M.W., Fleming, R.H., 1942. The Oceans: Their Physics, Chemistry and General Biology. Prentice Hall, Englewood Cliffs, NJ. 1087 pp.

Swenson, M.S., Niiler, P.P., 1996. Statistical analysis of the surface circulation of the California Current. J. Geophys. Res. Oceans 101 (C10), 22631–22645.

Swenson, M.S., Niiler, P.P., Brink, K.H., Abbott, M.R., 1992. Drifter observations of a cold filament off point Arena, California, in July 1988. J. Geophys. Res. 97 (C3), 3593–3610.

Sybrandy, A.L., Niiler, P.P., 1991. WOCE/TOGA Lagrangian drifter construction manual. WOCE Rep. 63, SIO Ref. 91/6. Scripps Institution of Oceanography, La Jolla, CA, 58 pp.

Sybrandy, A.L., Niiler, P.P., Martin, C., Scuba, W., Charpentier, E., Meldrum, D.T., 1992. Global Drifter Program Barometer Drifter Design Reference. Data Buoy Cooperation Panel Report 4, Revision 1.3 (December 2003).

Tapley, B.D., Bettadpur, S., Watkins, M., Reigber, C., 2004. The gravity recovery and climate experiment: mission overview and early results. Geophys. Res. Lett. 31, L09607. http://dx.doi.org/10.1029/2004GL019920.

Thomson, C.W., 1877. A Preliminary Account of the General Results of the Voyage of the HMS Challenger. MacMillan, London.

Thorpe, S.A., 2005. The Turbulent Ocean. Section 9.4. Langmuir Circulation. In: Cambridge University Press, pp. 251–257.

Uchida, U., Imawaki, S., 2003. Eulerian mean surface velocity field derived by combining drifter and satellite altimeter data. Geophys. Res. Lett. 30, 1229. http://dx.doi.org/10.1029/2002GL016445.

Uchida, H., Imawaki, S., Hu, J.-H., 1998. Comparison of Kuroshio surface velocities derived from satellite altimeter and drifting buoy data. J. Oceanogr. 54, 115–122.

Vélez-Belchí, P., Centurioni, L.R., Lee, D.-K., Jan, S., Niiler, P.P., 2013. Eddy induced Kuroshio intrusions onto the continental shelf of the East China Sea. J. Mar. Res. 71, 83–107.

Willis, J.K., Chambers, D.P., Kuo, C.-Y., Shum, C.K., 2010. Global sea level rise: recent progress and challenges for the decade to come. Oceanography 23 (4), 26–35. http://dx.doi.org/10.5670/oceanog.2010.03.

Winant, C.D., Alden, D.J., Dever, E.P., Edwards, K.A., Hendershott, M.C., 1999. Near-surface trajectories off central and southern California. J. Geophys. Res. 104 (C7), 15713–15726.

Wooster, W.S., Bakun, A., Mclain, D.R., 1976. Seasonal upwelling cycle along Eastern Boundary of North-Atlantic. J. Mar. Res. 34 (2), 131–141.

World Climate Research Program, 1988. WOCE surface velocity program planning committee report of first meeting: SVP-1 and TOGA pan-Pacific surface current study. WMO/TD-No.323, WCRP-26. World Meteorological Organization, Wormley, 33 pp.

Wunsch, C., Heimbach, P., Ponte, R.M., Fukumori, I., the ECCO-GODAE Consortium Members, 2009. The global general circulation of the ocean estimated by the ECCO-Consortium. Oceanography 22 (2), 88–103. http://dx.doi.org/10.5670/oceanog.2009.41.

Xie, S.-P., Liu, W.T., Liu, Q., Nonaka, M., 2001. Far-reaching effects of the Hawaiian islands on the Pacific ocean-atmosphere system. Science 292, 2057–2060.

Yaremchuk, M., Qu, T.D., 2004. Seasonal variability of the large-scale currents near the coast of the Philippines. J. Phys. Oceanogr. 34 (4), 844–855.

Zhang, D.X., Lee, T.N., Johns, W.E., Liu, C.T., Zantopp, R., 2001. The Kuroshio east of Taiwan: modes of variability and relationship to interior ocean mesoscale eddies. J. Phys. Oceanogr. 31 (4), 1054–1074.

Zhang, H.-M., Reynolds, R.W., Lumpkin, R., Molinari, R., Arzayus, K., Johnson, M., Smith, T.M., 2009. An integrated global observing system for sea surface temperature using satellites and in situ data: research to operations. Bull. Am. Meteorol. Soc. 90 (1), 31–38.